

## Chapter 1

### The International Linear Collider

Marco Battaglia

*Department of Physics, University of California at Berkeley and  
Lawrence Berkeley National Laboratory  
Berkeley, CA 94720, USA  
MBattaglia@lbl.gov*

The International Linear Collider (ILC) is the next large scale project in accelerator particle physics. Colliding electrons with positrons at energies from 0.3 TeV up to about 1 TeV, the ILC is expected to provide the accuracy needed to complement the LHC data and extend the sensitivity to new phenomena at the high energy frontier and answer some of the fundamental questions in particle physics and in its relation to Cosmology. This paper reviews some highlights of the ILC physics program and of the major challenges for the accelerator and detector design.

#### 1.1. Introduction

Accelerator particle physics is completing a successful cycle of precision tests of the Standard Model of electro-weak interactions (SM). After the discovery of the  $W$  and  $Z$  bosons at the  $Spp\bar{S}$  hadron collider at CERN, the concurrent operation of hadron and  $e^+e^-$  colliders has provided a large set of precision data and new observations. Two  $e^+e^-$  colliders, the SLAC Linear Collider (SLC) at the Stanford Linear Accelerator Center (SLAC) and the Large Electron Positron (LEP) collider at the European Organization for Nuclear Research (CERN), operated throughout the 1990's and enabled the study of the properties of the  $Z$  boson in great detail. Operation at LEP up to 209 GeV, the highest collision energy ever achieved in electron-positron collisions, provided detailed information on the properties of  $W$  bosons and the strongest lower bounds on the mass of the Higgs boson and of several supersymmetric particles. The collision of point-like, elementary particles at a well-defined and tunable energy offers advantages for

precision measurements, as those conducted at LEP and SLC, over proton colliders. On the other hand experiments at hadron machines, such as the Tevatron  $p\bar{p}$  collider at Fermilab, have enjoyed higher constituent energies. The CDF and D0 experiments eventually observed the direct production of top quarks, whose mass had been predicted on the basis of precision data obtained at LEP and SLC.

While we await the commissioning and operation of the LHC  $pp$  collider at CERN, the next stage in experimentation at lepton colliders is actively under study. For more than two decades, studies for a high-luminosity accelerator, able to collide electrons with positrons at energies of the order of 1 TeV, are being carried out world-wide.

## 1.2. The path towards the ILC

The concept of an  $e^+e^-$  linear collider dates back to a paper by Maury Tigner<sup>1</sup> published in 1965, when the physics potential of  $e^+e^-$  collisions had not yet been appreciated in full. This seminal paper envisaged collisions at 3-4 GeV with a luminosity competitive with that of the SPEAR ring at SLAC, i.e.  $3 \times 10^{30} \text{ cm}^{-2} \text{ s}^{-1}$ . A possible scheme to obtain  $e^-e^-$  and  $e^+e^-$  collisions at energies of hundreds of GeV is the title of a paper<sup>2</sup> by Ugo Amaldi published a decade later in 1976, which sketches the linear collider concept with a design close to that now developed for the ILC. The

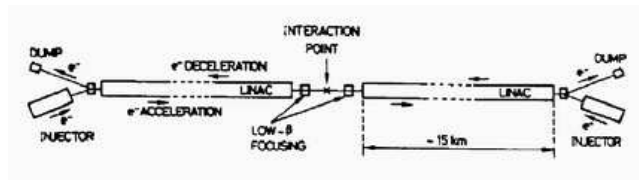


Fig. 1.1. The linear collider layout as sketched in 1975 in one of the figures of Ref.<sup>2</sup> The paper discussed the possibility to achieve  $e^-e^-$  and  $e^+e^-$  collisions at 0.3 TeV using superconducting linacs with a gradient of 10 MV/m.

parameters for a linear collider, clearly recognised as the successors of  $e^+e^-$  storage rings on the way to high energies, were discussed by Burt Richter at the IEEE conference in San Francisco in 1979<sup>3</sup> and soon after came the proposal for the *Single Pass Collider Project* which would become SLC at SLAC.

From 1985, the CERN Long Range Planning Committee considered an  $e^+e^-$  linear collider, based on the CLIC<sup>4</sup> design, able to deliver collisions

at 2 TeV with  $10^{33} \text{ cm}^{-2} \text{ s}^{-1}$  luminosity, *vis-a-vis* a hadron collider, with proton-proton collisions at 16 TeV and luminosity of  $1.4 \times 10^{33} \text{ cm}^{-2} \text{ s}^{-1}$ , as a candidate for the new CERN project after LEP. That review process eventually led to the decision to build the LHC, but it marked an important step to establish the potential of a high energy  $e^+e^-$  collider. It is important to note that it was through the contributions of several theorists, including John Ellis, Michael Peskin, Gordon Kane and others, that the requirements in terms of energy and luminosity for a linear collider became clearer in the mid 1980's.<sup>5</sup> The SLC project gave an important proof of principle for a high energy linear collider and the experience gained has shaped the subsequent designs in quite a significant way.

After a decade marked by important progress in the R&D of the basic components and the setup of advanced test facilities, designs of four different concepts emerged: TESLA, based on superconducting RF cavities, the NLC/JLC-X, based on high frequency (11.4 GHz) room-temperature copper cavities, JLC-C, based on lower frequency (5.7 GHz) conventional cavities and CLIC, a multi-TeV collider based on a different beam acceleration technique, the two-beam scheme with transfer structures operating at 30 GHz. Accelerator R&D had reached the maturity to assess the technical feasibility of a linear collider project and take an informed choice of the most advantageous RF technology. The designs were considered by the International Linear Collider Technical Review Committee (ILC-TRC), originally formed in 1994 and re-convened by the International Committee for Future Accelerators (ICFA) in 2001 under the chairmanship of Greg A. Loew. The ILC-TRC assessed their status using common criteria, identified outstanding items needing R&D effort and suggested areas of collaboration. The TRC report was released in February 2003<sup>6</sup> and the committee found that there were *no insurmountable show-stoppers to build TESLA, NLC/JLC-X or JLC-C in the next few years and CLIC in a more distant future, given enough resources*. Nonetheless, significant R&D remained to be done. At this stage, it became clear that, to make further progress, the international effort towards a linear collider should be focused on a single design. ICFA gave mandate to an International Technology Recommendation Panel (ITRP), chaired by Barry Barish, to make a definite recommendation for a RF technology that would be the basis of a global project. In August 2004 the ITRP made the recommendation in favour of superconducting RF cavities.<sup>7</sup> The technology choice, which was promptly accepted by all laboratories and groups involved in the R&D process, is regarded as a major step towards the realization of the linear collider project. Soon after it, a

truly world-wide, centrally managed design effort, the Global Design Effort (GDE),<sup>8</sup> a team of more than 60 persons, started, with the aim to produce an ILC Reference Design Report by beginning of 2007 and an ILC Technical Design Report by end of 2008. The GDE responsibility now covers the detailed design concept, performance assessments, reliable international costing, industrialization plan, siting analysis, as well as detector concepts and scope. A further important step has been achieved with release of the Reference Design Report in February 2007.<sup>9</sup> This report includes a preliminary value estimate of the cost for the ILC in its present design and at the present level of engineering and industrialisation. The value estimate is structured in three parts: 1.78 Billion ILC Value Units for site-related costs, such as those of tunneling in a specific region, 4.87 Billion ILC Value Units for the value of the high technology and conventional components and 13,000 person-years for the required supporting manpower. For this estimate the conversion factor is 1 ILC Value Unit = 1 US Dollar = 0.83 Euro = 117 Yen. This estimate, which is comparable to the LHC cost, when the pre-existing facilities, such as the LEP tunnel, are included, provides guidance for optimisation of both the design and the R&D to be done during the engineering phase, due to start in Fall 2007.

Technical progress was paralleled by increasing support for the ILC in the scientific community. At the 2001 APS workshop *The Future of Physics* held in Snowmass, CO, a consensus emerged for the ILC as the right project for the next large scale facility in particle physics. This consensus resonated and expanded in a number of statements by highly influential scientific advisory panels world-wide. The ILC role in the future of scientific research was recognised by the OECD Consultative Group on High Energy Physics,<sup>10</sup> while the DOE Office of Science ranked the ILC as its top mid-term project. More recently the EPP 2010 panel of the US National Academy of Sciences, in a report titled *Elementary Particle Physics in the 21<sup>st</sup> Century* has endorsed the ILC as the next major experimental facility to be built and its role in elucidating the physics at the high energy frontier, independently from the LHC findings.<sup>11</sup> Nowadays, the ILC is broadly regarded as the highest priority for a future large facility in particle physics, needed to extend and complement the LHC discoveries with the accuracy which is crucial to understand the nature of New Physics, test fundamental properties at the high energy scale and establish their relation to other fields in physical sciences, such as Cosmology. A matching program of physics studies and detector R&D efforts has been in place for the past decade and it is now developing new, accurate and cost effective detector designs from

proof of concepts towards that stage of engineering readiness, needed for being adopted in the ILC experiments.

### 1.3. ILC Accelerator Parameters

#### 1.3.1. *ILC Energy*

The first question which emerges in defining the ILC parameters is the required centre-of-mass energy  $\sqrt{s}$ . It is here where we most need physics guidance to define the next thresholds at, and beyond, the electro-weak scale. The only threshold which, at present, is well defined numerically is that of top-quark pair production at  $\sqrt{s} \simeq 350$  GeV. Beyond it, there is a strong prejudice, supported by precision electro-weak and other data, that the Higgs boson should be light and new physics thresholds may exist between the electro-weak scale and approximately 1 TeV. If indeed the SM Higgs boson exists and the electro-weak data is not affected by new physics, its mass  $M_H$  is expected to be below 200 GeV as discussed in section 1.4.1. Taking into account that the Higgs main production process is in association with a  $Z^0$  boson, the maximum of the  $e^+e^- \rightarrow H^0Z^0$  cross section varies from  $\sqrt{s} = 240$  GeV to 350 GeV for  $120 \text{ GeV} < M_H < 200 \text{ GeV}$ . On the other hand, we know that the current SM needs to be extended by some New Physics. Models of electroweak symmetry breaking contain new particles in the energy domain below 1 TeV. More specifically, if Supersymmetry exists and it is responsible for the dark matter observed in the Universe, we expect that a significant fraction of the supersymmetric spectrum would be accessible at  $\sqrt{s} = 0.5\text{-}1.0$  TeV. In particular, the ILC should be able to study in detail those particles determining the dark matter relic density in the Universe by operating at energies not exceeding 1 TeV, as discussed in section 1.4.2. Another useful perspective on the ILC energy is an analysis of the mass scale sensitivity for new physics vs. the  $\sqrt{s}$  energy for lepton and hadron colliders in view of their synergy. The study of electro-weak processes at the highest available energy offers a window on mass scales well beyond its kinematic reach. A comparison of the mass-scale sensitivity for various new physics scenarios as a function of the centre-of-mass energy for  $e^+e^-$  and  $pp$  collisions is given in section 1.4.3. These and similar considerations, emerged in the course of the world-wide studies on physics at the ILC, motivate the choice of  $\sqrt{s} = 0.5$  TeV as the reference energy parameter, but requiring the ILC to be able to operate, with substantial luminosity, at 0.3 TeV as well and to be upgradable up to approximately

6

1 TeV.

It is useful to consider these energies in an historical perspective. In 1954 Enrico Fermi gave a talk at the American Physical Society, of which he was chair, titled *What can we learn with high energy accelerators ?*. In that talk Fermi considered a proton accelerator with a radius equal to that of Earth and 2 T bending magnets, thus reaching a beam energy of  $5 \times 10^{15}$  eV.<sup>12</sup> Stanley Livingstone, who had built with Ernest O. Lawrence the first circular accelerator at Berkeley in 1930, had formulated an empirical linear scaling law for the available centre-of-mass energy vs. the construction year and cost. Using Livingstone curve, Fermi predicted that such an accelerator could be built in 1994 at a cost of 170 billion \$. We have learned that, not only such accelerator could not be built, but accelerator physics has irrevocably fallen off the Livingstone curve, even in its revised version, which includes data up to the 1980's. As horizons expanded, each step has involved more and more technical challenges and has required more resources. The future promises to be along this same path. This underlines the need of coherent and responsible long term planning while sustaining a rich R&D program in both accelerator and detector techniques.

The accelerator envisaged by Enrico Fermi was a circular machine, as the almost totality of machines operating at the high energy frontier still are. Now, as it is well known, charged particles undergoing a centripetal acceleration  $a = v^2/R$  radiate at rate  $P = \frac{1}{6\pi\epsilon_0} \frac{e^2 a^2}{c^3} \gamma^4$ . If the radius  $R$  is kept constant, the energy loss is the above rate  $P$  times  $t = 2\pi R/v$ , the time spent in the bending section of the accelerator. The energy loss for electrons is  $W = 8.85 \times 10^{-5} \frac{E^4(\text{GeV}^4)}{R(\text{km})}$  MeV per turn while for protons is  $W = 7.8 \times 10^{-3} \frac{E^4(\text{TeV}^4)}{R(\text{km})}$  keV per turn. Since the energy transferred per turn by the RF cavities to the beam is constant,  $G \times 2R \times F$ , where  $G$  is the cavity gradient and  $F$  the tunnel fill factor, for each value of the accelerator ring radius  $R$  there exists a maximum energy  $E_{max}$  beyond which the energy loss exceeds the energy transferred. In practice, before this value of  $E_{max}$  is reached, the real energy limit is set by the power dumped by the beam as synchrotron radiation. To make a quantitative example, in the case of the LEP ring, with a radius  $R = 4.3$  km, a beam of energy  $E_{beam} = 250$  GeV, would lose 80 GeV/turn. Gunther Voss is thought to be the author of a plot comparing the guessed cost of a storage ring and a linear collider as a function of the  $e^+e^-$  centre-of-mass energy. A  $\sqrt{s} = 500$  GeV storage ring, which would have costed an estimated 14 billions CHF in 1970's is aptly labelled as the Crazytron.<sup>13</sup> LEP filled the last window of

opportunity for a storage ring at the high energy frontier. Beyond LEP-2 energies the design must be a linear collider, where no bending is applied to the accelerated particles. Still the accelerator length is limited by a number of constraints which include costs, alignment and siting. Therefore, technology still defines the maximum reachable energy at the ILC.

The ILC design is based on superconducting (s.c.) radio-frequency (RF) cavities. While s.c. cavities had been considered already in the 1960's, it was Ugo Amaldi to first propose a fully s.c. linear collider in 1975.<sup>2</sup> By the early

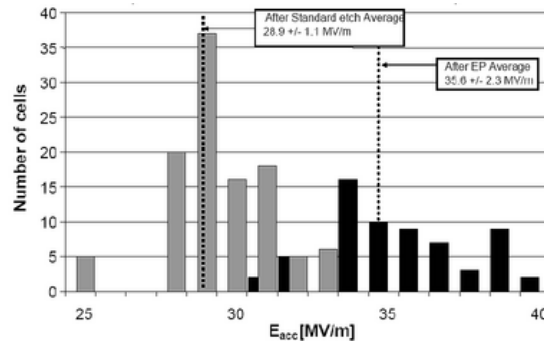


Fig. 1.2. Distributions of gradients measured for pure niobium, nine-cell cavities. After electro-polishing an average gradient in excess to 35 MV/m has been obtained.

1990's, s.c. cavities equipped already one accelerator, TRISTAN at KEK in Japan, while two further projects were in progress, CEBAF at Cornell and the LEP-2 upgrade at CERN. LEP-2 employed a total of 288 s.c. RF cavities, providing an average gradient of 7.2 MV/m. It was the visionary effort of Bjorn Wijk to promote, from 1990, the TESLA collaboration, with the aim to develop s.c. RF cavities pushing the gradient higher by a factor of five and the production costs down by a factor of four, thus reducing the cost per MV by a factor of twenty. Such reduction in cost was absolutely necessary to make a high energy collider, based on s.c. cavities, feasible. Within less than a decade 1.3 GHz, pure niobium cavities achieved gradients in excess to 35 MV/m. This opened the way to their application to a  $e^+e^-$  linear collider, able to reach centre-of-mass energies of the order of 1 TeV, as presented in detail in the TESLA proposal published in 2001<sup>14</sup> and recommended for the ILC by the ITRP in 2004.<sup>7</sup>

Today, the ILC baseline design aims at matching technical feasibility to cost optimisation. One of the major goals of the current effort in the ILC design is to understand enough about its costs to provide a reliable

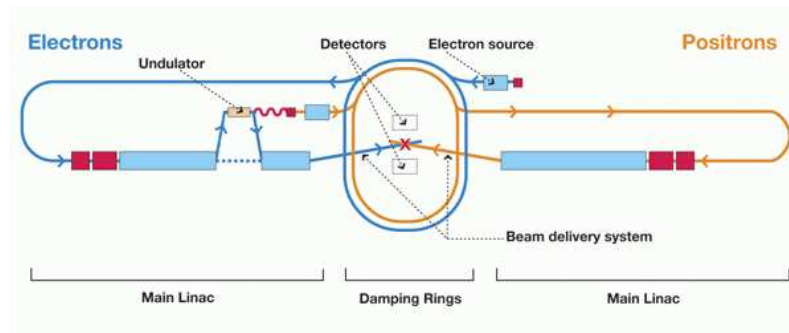


Fig. 1.3. Schematic layout of the International Linear Collider. This diagram reflects the recommendations of the Baseline Configuration Document, a report published in December 2005 that outlines the general design of the machine. (Credit ILC Global Design Effort)

indication of the scale of funding required to carry out the ILC project. Preparing a reliable cost estimate for a project to be carried out as a truly world-wide effort at the stage of a conceptual design that still lacks much of the detailed engineering designs as well as agreements for responsibility and cost sharing between the partners and a precise industrialisation plan is a great challenge. Still having good cost information as soon as possible, to initiate negotiations with the funding agencies is of great importance. An interesting example of the details entering in this process is the optimisation of the cost vs. cavity gradient for a 0.5 TeV collider. The site length scales inversely with the gradient  $G$  while the cost of the cryogenics scales as  $G^2/Q_0$  resulting in a minimum cost for a gradient of 40 MW/m, corresponding to a tunnel length of 40 km, and a fractional cost increase of 10 % for gradients of 25 MV/m or 57 MV/m. The chosen gradient of 35 MV/m, which is matched by the average performance of the most recent prototypes after electro-polishing, gives a total tunnel length of 44 km with a cost increment from the minimum of just 1 %.

Beyond 1 TeV, the extension of conventional RF technology is more speculative. In order to attain collisions at energies in excess of about 1 TeV, with high luminosity, significantly higher gradients are necessary. As the gradient of s.c. cavities is limited below  $\sim 50$  MV/m, other avenues should be explored. The CLIC technology,<sup>15</sup> currently being developed at CERN and elsewhere, may offer gradients of the order of 150 MV/m,<sup>16</sup> allowing collision energies in the range 3-5 TeV with a luminosity of  $10^{35}$  cm<sup>-2</sup> s<sup>-1</sup>, which would support a compelling physics pro-



gram.<sup>17</sup> While RF cavities are limited to accelerating fields of order of

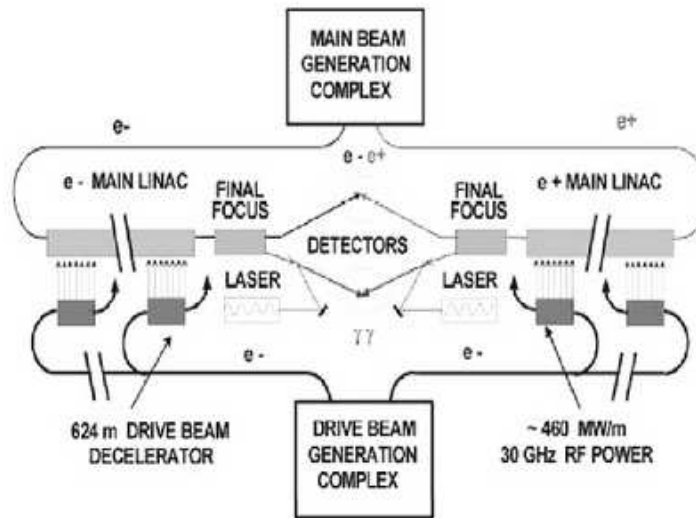


Fig. 1.4. Schematics of the overall layout of the CLIC complex for  $e^+e^-$  collisions at  $\sqrt{s} = 3$  TeV. (from Ref<sup>17</sup>)

100-200 MV/m, or below, laser-wakefield accelerators are capable, in principle, of producing fields of 10-100 GV/m. Recently a 1 GeV  $e^-$  beam has been accelerated over just 3.3 cm using a 40 TW peak-power laser pulse,<sup>18</sup> thus opening a possible path towards ultra-high energies in  $e^+e^-$  collisions in some more distant future.

### 1.3.2. ILC Luminosity

The choice of a linear collider, rather than a circular storage ring, while solving the problem of the maximum reachable energy, introduces the challenge of achieving collisions with the required luminosity. The luminosity,  $\mathcal{L}$ , defined as the proportionality factor between the number of events produced and the process cross section  $\sigma$ , has requirements which depend on the typical values of s-channel cross sections and so scale as  $1/s$ . First luminosity requirements were already outlined in the 1980s<sup>19,20</sup> as  $\mathcal{L} \simeq \frac{2E_{beam}}{\text{TeV}} \times 10^{33} \text{ cm}^{-2} \text{ s}^{-1}$ , based on the estimated discovery potential. But in the present vision of the ILC role in probing the high energy frontier new requirements must be considered. One example is the precision study

of electro-weak processes to look for deviations from the SM predictions, due to effect of new physics at high scales. The  $e^+e^- \rightarrow b\bar{b}$  cross section at 1 TeV is just 96 fb, so this would corresponds to less than  $10^3$  events per year at  $10^{33} \text{ cm}^{-2} \text{ s}^{-1}$ , which is certainly insufficient for the kind of precision measurements which we expect from the ILC. Another example is offered by one of the reactions most unique to the ILC: the double-Higgs production  $e^+e^- \rightarrow HHZ$  sensitive to the Higgs self-coupling, which has a cross section of order of only 0.2 fb at 0.5 TeV. Therefore a luminosity of  $10^{34} \text{ cm}^{-2} \text{ s}^{-1}$  or more is required as baseline parameter.

The luminosity can be expressed as a function of the accelerator parameters as:

$$\mathcal{L} = f_{rep} n_b \frac{N^2}{4\pi\sigma_x\sigma_y}. \quad (1.1)$$

Now, since in a linear machine the beams are collided only once and then dumped, the collision frequency,  $f_{rep}$ , is small and high luminosity should be achieved by increasing the number of particles in a bunch  $N$ , the number of bunches  $n_b$  and decreasing the transverse beam size  $\sigma$ . Viable values for  $N$  are limited by wake-field effects and the ILC parameters have the same number of electrons in a bunch as LEP had, though it aims at a luminosity three orders of magnitude higher. Therefore, the increase must come from a larger number of bunches and a smaller transverse beam size. The generation of beams of small transverse size, their preservation during acceleration and their focusing to spots of nanometer size at the interaction region presents powerful challenges which the ILC design must solve. A small beam size also induces beam-beam interactions. On one hand the beam self-focusing, due to the electrostatic attraction of particles of opposite charges enhances the luminosity. But beam-beam interactions also result in an increase of beamstrahlung with a larger energy spread of the colliding particles, a degraded luminosity spectrum and higher backgrounds. Beamstrahlung is energy loss due to particle radiation triggered by the trajectory bending in the interactions with the charged particles in the incoming bunch.<sup>21</sup> The mean beamstrahlung energy loss, which has to be minimised, is given by:

$$\delta_{BS} \simeq 0.86 \frac{er_e^3}{2m_0c^2} \frac{E_{cm}}{\sigma_z} \frac{N_b^2}{(\sigma_x + \sigma_y)^2}. \quad (1.2)$$

Since the luminosity scales as  $\frac{1}{\sigma_x\sigma_y}$ , while the beamstrahlung energy loss scales as  $\frac{1}{\sigma_x + \sigma_y}$ , it is advantageous to choose a large beam aspect ratio,

with the vertical beam size much smaller than the horizontal component. The parameter optimisation for luminosity can be further understood by expressing the luminosity in terms of beam power  $P = f_{rep} N E_{cm} = \eta P_{AC}$  and beamstrahlung energy loss as:

$$\mathcal{L} \propto \frac{\eta P_{AC}}{E_{cm}} \sqrt{\frac{\delta_{BS}}{\epsilon_y}} H_D \quad (1.3)$$

which highlights the dependence on the cavity efficiency  $\eta$  and the total power  $P_{AC}$ . The  $H_D$  term is the pinch enhancement factor, that accounts for the bunch attraction in the collisions of oppositely charged beams. In summary, since the amount of available power is necessarily limited, the main handles on luminosity are  $\eta$  and  $\epsilon_y$ . The efficiency for transferring power from the plug to the beam is naturally higher for s.c. than for conventional copper cavities, so more relaxed collision parameters can be adopted for a s.c. linear collider delivering the same luminosity. The main beam parameters for the ILC baseline design are given in Table 1.1.

Table 1.1. ILC baseline design beam parameters

Parameter	$\sqrt{s}$	$\sqrt{s}$
	0.5 TeV	1.0 TeV
Luminosity $L$ ( $10^{34} \text{ cm}^{-2} \text{ s}^{-1}$ )	2.0	2.8
Frequency (Hz)	5.0	5.0
Nb. of particles ( $10^{10}$ )	2.0	2.0
Nb. of bunches $N_b$	2820	2820
Bunch spacing (ns)	308	308
Vertical beam size $\sigma_y$ (nm)	5.7	3.5
Beamstrahlung Parameter $\delta_{BS}$	0.022	0.050
$H_D$	1.7	1.5

#### 1.4. ILC Physics Highlights

The ILC physics program, as we can anticipate it at present, is broad and diverse, compelling and challenging. The ILC is being designed for operation at 0.5 TeV with the potential to span the largest range of collision energies, from the  $Z^0$  peak at 0.091 TeV up to 1 TeV, collide electrons with positrons, but optionally also electrons with electrons, photons with photons and photons with electrons, and combine various polarization states of the electron and positron beams. Various reports discussing the linear collider physics case, including results of detailed physics studies, have been

published in the last few years.<sup>5,17,22–26</sup> Here, I shall focus on three of the main ILC physics themes: the detailed study of the Higgs boson profile, the determination of neutralino dark matter density in the Universe from accelerator data, and the sensitivity to new phenomena beyond the ILC kinematic reach, through the analysis of two-fermion production, at the highest  $\sqrt{s}$  energy. Results discussed in the following have been obtained mostly using realistic, yet parametric simulation of the detector response. Only few analyses have been carried out which include the full set of physics and machine-induced backgrounds on fully simulated and reconstructed events. With the progress of the activities of detector concepts and the definition of well-defined benchmark processes, this is becoming one of the priorities for the continuation of physics and detector studies.

#### 1.4.1. *The Higgs Profile at the ILC*

Explaining the origin of mass is one of the great scientific quests of our time. The SM addresses this question by the Higgs mechanism.<sup>27</sup> The first direct manifestation of the Higgs mechanism through the Higgs sector will be the existence of at least one Higgs boson. The observation of a new spin-0 particle would represent a first sign that the Higgs mechanism of mass generation is indeed realised in Nature. This has motivated a large experimental effort, from LEP-2 to the Tevatron and, soon, the LHC, actively backed-up by new and more accurate theoretical predictions. After a Higgs discovery, which we anticipate will be possible at the LHC, full validation of the Higgs mechanism can only be established by an accurate study of the Higgs boson production and decay properties. It is here where the ILC potential in precision physics will be crucial for the validation of the Higgs mechanism, through a detailed study of the Higgs profile.<sup>31</sup>

The details of this study depend on the Higgs boson mass,  $M_H$ . In the SM,  $M_H = \sqrt{2\lambda}v$  where the Higgs field expectation value  $v$  is determined as  $(\sqrt{2}G_F)^{-1/2} \approx 246$  GeV, while the Higgs self-coupling  $\lambda$  is not specified, leaving the mass as a free parameter. However, we have strong indications that  $M_H$  must be light. The Higgs self-coupling behaviour at high energies,<sup>28</sup> the Higgs field contribution to precision electro-weak data<sup>30</sup> and the results of direct searches at LEP-2<sup>29</sup> at  $\sqrt{s} \geq 206$  GeV, all point towards a light Higgs boson. In particular, the study of precision electro-weak data, which are sensitive to the Higgs mass logarithmic contribution to radiative corrections, is based on several independent observables, including masses ( $m_{top}$ ,  $M_W$ ,  $M_Z$ ), lepton and quark asymmetries at the  $Z^0$  pole,  $Z^0$  line-

shape and partial decay widths. The fit to eighteen observables results in a 95% C.L. upper limit for the Higgs mass of 166 GeV, which becomes 199 GeV when the lower limit from the direct searches at LEP-2,  $M_H > 114.4$  GeV, is included. As a result, current data indicates that the Higgs boson mass should be in the range  $114 \text{ GeV} < M_H < 199 \text{ GeV}$ . It is encouraging to observe that if the same fit is repeated, but excluding this time  $m_{top}$  or  $M_W$ , the results for their values,  $178_{-9}^{+12}$  GeV and  $80.361 \pm 0.020$  GeV respectively, are in very good agreement with the those obtained the direct determinations,  $m_{top} = 171.4 \pm 2.1$  GeV and  $M_W = 80.392 \pm 0.029$  GeV.

At the ILC the Higgs boson can be observed in the Higgs-strahlung production process  $e^+e^- \rightarrow HZ$  with  $Z \rightarrow \ell^+\ell^-$ , independent of its decay mode, by the distinctive peak in the di-lepton recoil mass distribution. A data set of  $500 \text{ fb}^{-1}$  at  $\sqrt{s} = 350$  GeV, corresponding to four years of ILC running, provides a sample of 3500-2200 Higgs particles produced in the di-lepton  $HZ$  channel, for  $M_H = 120$ -200 GeV. Taking into account the SM backgrounds, dominated by  $e^+e^- \rightarrow Z^0Z^0$  and  $W^+W^-$  production, the Higgs boson observability is guaranteed up to its production kinematical limit, independent of its decays. This sets the ILC aside from the LHC, since the ILC sensitivity to the Higgs boson does not depend on its detailed properties.

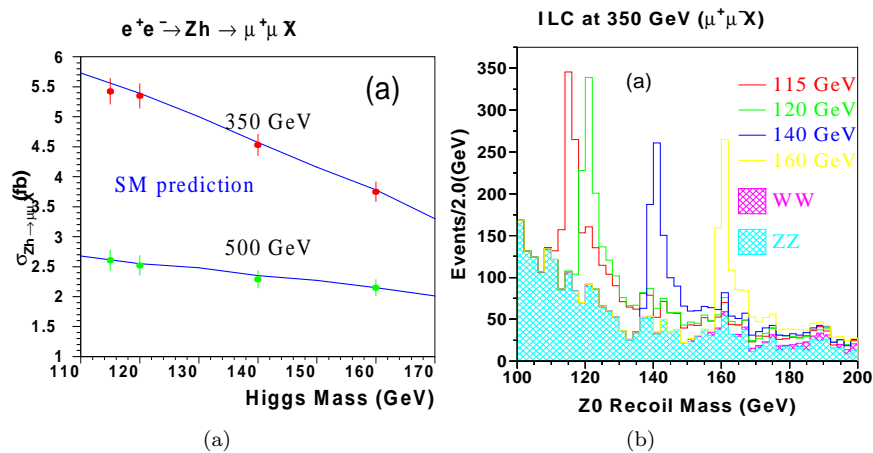


Fig. 1.5. The Higgs-strahlung process at the ILC. (a)  $e^+e^- \rightarrow HZ$  cross section vs.  $M_H$  for  $\sqrt{s} = 0.35$  TeV and 0.5 TeV, (b) reconstructed  $\mu^+\mu^-$  recoil mass for various values of the Higgs boson mass (Credit: ALCPG Study Group).

After observation of a new particle with properties compatible with those of the Higgs boson, a significant experimental and theoretical effort will be needed to verify that this is indeed the boson of the scalar field responsible for the electro-weak symmetry breaking and the generation of mass. Outlining the Higgs boson profile, through the determination of its mass, width, quantum numbers, couplings to gauge bosons and fermions and the reconstruction of the Higgs potential, stands as a most challenging, yet compelling, physics program. The ILC, with its large data sets at different centre-of-mass energies and beam polarisation conditions, the high resolution detectors providing unprecedented accuracy on the reconstruction of the event properties and the use of advanced analysis techniques, developed from those successfully adopted at LEP and SLC, promises to promote Higgs physics into the domain of precision measurements. Since the Higgs mass  $M_H$  is not predicted by theory, it is of great interest to measure it precisely. Once this mass, and thus  $\lambda$ , is fixed, the profile of the Higgs particle is uniquely determined in the SM. In most scenarios we expect the LHC to determine the Higgs mass with a good accuracy. At the ILC, this measurement can be refined by exploiting the kinematical characteristics of the Higgs-strahlung production process  $e^+e^- \rightarrow Z^* \rightarrow H^0 Z^0$  where the  $Z^0$  can be reconstructed in both its leptonic and hadronic decay modes. The  $\ell^+\ell^-$  recoil mass for leptonic  $Z^0$  decays yields an accuracy of 110 MeV for  $500 \text{ fb}^{-1}$  of data, without any requirement on the nature of the Higgs decays. Further improvement can be obtained by explicitly selecting  $H \rightarrow b\bar{b}$  ( $WW$ ) for  $M_H \leq (>) 140 \text{ GeV}$ . Here a kinematical 5-C fit, imposing energy and momentum conservation and the mass of a jet pair to correspond to  $M_Z$ , achieves an accuracy of 40 to 90 MeV for  $120 < M_H < 180 \text{ GeV}$ .<sup>32</sup>

The total decay width of the Higgs boson is predicted to be too narrow to be resolved experimentally for Higgs boson masses below the  $ZZ$  threshold. On the contrary, above  $\simeq 200 \text{ GeV}$ , the total width can be measured directly from the reconstructed width of the recoil mass peak, as discussed below. For the lower mass range, indirect methods must be applied. In general, the total width is given by  $\Gamma_{tot} = \Gamma_X / \text{BR}(H \rightarrow X)$ . Whenever  $\Gamma_X$  can be determined independently of the corresponding branching fraction, a measurement of  $\Gamma_{tot}$  can be carried out. The most convenient choice is the extraction of  $\Gamma_H$  from the measurements of the  $WW$  fusion cross section and the  $H \rightarrow WW^*$  decay branching fraction. A relative precision of 6% to 13% on the width of the Higgs boson can be obtained at the ILC with this technique, for masses between 120 GeV and 160 GeV. The spin, parity

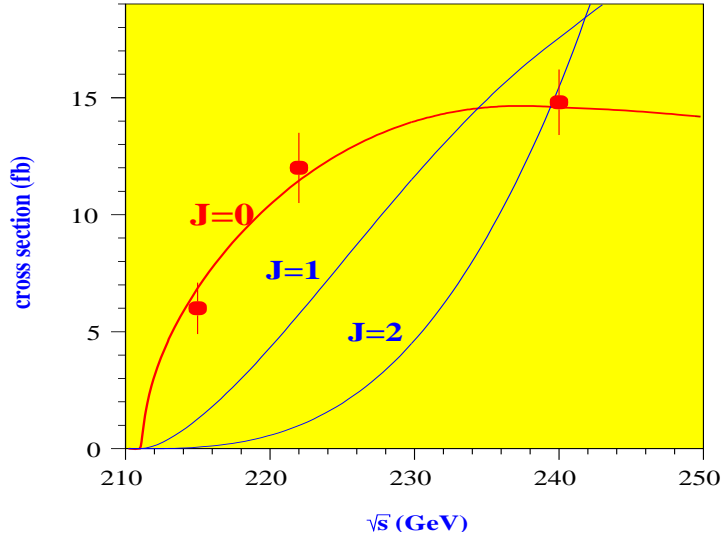


Fig. 1.6. Determination of the Higgs boson spin from a scan of the  $e^+e^- \rightarrow HZ$  cross section at threshold at the ILC (from Ref<sup>23</sup>).

and charge-conjugation quantum numbers  $J^{PC}$  of Higgs bosons can be determined at the ILC in a model-independent way. Already the observation of either  $\gamma\gamma \rightarrow H$  production or  $H \rightarrow \gamma\gamma$  decay sets  $J \neq 1$  and  $C = +$ . The angular dependence  $\frac{d\sigma_{ZH}}{d\theta} \propto \sin^2 \theta$  and the rise of the Higgs-strahlung cross section:

$$\sigma_{ZH} \propto \beta \sim \sqrt{s - (M_H + M_Z)^2} \quad (1.4)$$

allows to determine  $J^P = 0^+$  and distinguish the SM Higgs from a  $CP$ -odd  $0^{-+}$  state  $A^0$ , or a  $CP$ -violating mixture of the two.<sup>33,34</sup> But where the ILC has a most unique potential is in verifying that the Higgs boson does its job of providing gauge bosons, quarks and leptons with their masses. This requires to precisely test the relation  $g_{HXX} \propto m_X$  between the Yukawa couplings,  $g_{HXX}$ , and the corresponding particle masses,  $m_X$ . In fact, the SM Higgs couplings to fermion pairs  $g_{Hff} = m_f/v$  are fully determined by the fermion mass  $m_f$ . The corresponding decay partial widths only depend on these couplings and on the Higgs boson mass, QCD corrections do not represent a significant source of uncertainty.<sup>35</sup> Therefore, their accurate determination will represent a comprehensive test of the Higgs mechanism of mass generation.<sup>36</sup> Further, observing deviations of the measured values

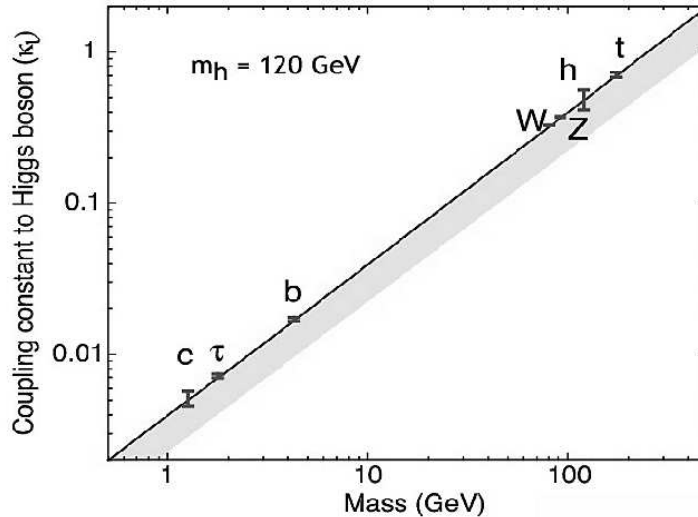


Fig. 1.7. Particle couplings to the Higgs field, for a 120 GeV boson, as a function of the particle masses. The error bars show the expected ILC accuracy in determining each of the couplings. The dark line is the SM prediction, while the shaded gray area shows the range of predictions from theories of new physics beyond the SM with extra dimensions (Credit: ACFA ILC Study Group).

from the SM predictions will probe the structure of the Higgs sector and may reveal a non-minimal implementation of the Higgs model or the effect of new physics inducing a shift of the Higgs couplings.<sup>37-39</sup> The accuracy of these measurements relies on the performances of jet flavour tagging and thus mostly on the Vertex Tracker, making this analysis an important benchmark for optimising the detector design. It is important to ensure that the ILC sensitivity extends over a wide range of Higgs boson masses and that a significant accuracy is achieved for most particle species. Here, the ILC adds the precision which establishes the key elements of the Higgs mechanism. It is important to point out that these tests are becoming more stringent now that the  $B$ -factories have greatly improved the determination of the  $b$ - and  $c$ -quark masses. When one of these studies was first presented in 1999,<sup>40</sup> the  $b$  quark mass was known to  $\pm 0.11$  GeV and the charm mass to  $\pm 0.13$  GeV, with the expectation that  $e^+e^-$   $B$ -factory and LHC data could reduce these uncertainties by a factor of two by the time the ILC data would be analysed. Today, the analysis of a fraction of the BaBar data<sup>41</sup> has already brought these uncertainties down to 0.07 GeV for



$m_b$  and, more importantly, 0.09 GeV for  $m_c$ , using the spectral moments technique in semi-leptonic  $B$  decays, which had been pioneered on CLEO<sup>42</sup> and DELPHI data.<sup>43</sup> Extrapolating to the anticipated total statistics to be collected at PEP-II and KEKB, we can now confidently expect that the  $b$  quark mass should be known to better than  $\pm 0.05$  GeV and the charm mass to better than  $\pm 0.06$  GeV. This translates into less than  $\pm 0.4$  % and  $\pm 6.5$  % relative uncertainty in computing the Higgs SM couplings to  $b$  and  $c$  quarks, respectively, and motivates enhanced experimental precision in the determination of these couplings at the ILC. Detailed simulation shows that these accuracy can be matched by the ILC.<sup>44,47</sup>

While much of the emphasis on the ILC capabilities in the study of the Higgs profile is for a light Higgs scenario, preferred by the current electro-weak data and richer in decay modes, the ILC has also the potential of precisely mapping out the Higgs boson properties for heavier masses. If the Higgs boson turns out to weigh of order 200 GeV, the 95% C.L. upper limit indicated by electro-weak fits, or even heavier, the analysis of the recoil mass in  $e^+e^- \rightarrow HZ$  at  $\sqrt{s} = 0.5$  TeV allows to precisely determine  $M_H$ ,  $\Gamma_H$  and the Higgs-strahlung cross section. Even for  $M_H = 240$  GeV, the mass can be determined to a  $10^{-3}$  accuracy and, more importantly, the total width measured about 10% accuracy. Decays of Higgs bosons produced in  $e^+e^- \rightarrow H\nu\bar{\nu}$  give access to the Higgs couplings. The importance of the  $WW$ -

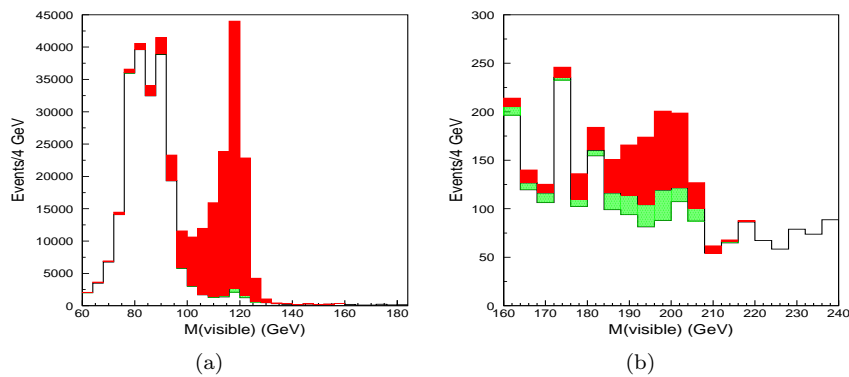


Fig. 1.8.  $H \rightarrow b\bar{b}$  signal after full event selection at the ILC for (a)  $M_H = 120$  GeV and (b)  $M_H = 200$  GeV (from Ref<sup>47</sup>).

fusion process  $e^+e^- \rightarrow H^0\nu\bar{\nu}$  to probe rare Higgs decays at higher energies, emerged in the physics study for a multi-TeV linear collider.<sup>45</sup> Since this

cross section increases as  $\log \frac{s}{M_H^2}$ , it becomes dominant around  $\sqrt{s} = 1$  TeV. Detailed studies have been performed and show that  $1 \text{ ab}^{-1}$  of data at  $\sqrt{s} = 1$  TeV, corresponding to three to four years of ILC running, can significantly improve the determination of the Higgs couplings, especially for the larger values of  $M_H$ .<sup>46,47</sup>  $WW$  and  $ZZ$  couplings can be determined with relative accuracies of 3 % and 5 % respectively, while the coupling to  $b\bar{b}$  pairs, a rare decay with a branching fraction of just  $2 \times 10^{-3}$  at such large masses, can be determined to 4 % to 14 % for  $180 \text{ GeV} < M_H < 220 \text{ GeV}$ . This measurement is of great importance, since it would offer the only opportunity to learn about the fermion couplings of such an heavy Higgs boson, and it is unique to a linear collider.

A most distinctive feature of the Higgs mechanism is the shape of the Higgs potential:

$$V(\Phi) = -\frac{\mu^2}{2}\Phi^2 + \frac{\lambda}{4}\Phi^4 \quad (1.5)$$

with  $v = \sqrt{\frac{\mu^2}{\lambda}}$ . In the SM, the triple Higgs coupling,  $g_{HHH} = 3\lambda v$ , is related to the Higgs mass,  $M_H$ , through the relation

$$g_{HHH} = \frac{3}{2} \frac{M_H^2}{v}. \quad (1.6)$$

By determining  $g_{HHH}$ , the above relation can be tested. The ILC has access to the triple Higgs coupling through the double Higgs production processes  $e^+e^- \rightarrow HHZ$  and  $e^+e^- \rightarrow HH\nu\nu$ .<sup>48</sup> Deviations from the SM relation for the strength of the Higgs self-coupling arise in models with an extended Higgs sector.<sup>49</sup> The extraction of  $g_{HHH}$  is made difficult by their tiny cross sections and by the dilution effect, due to diagrams leading to the same double Higgs final states, but not sensitive to the triple Higgs vertex. This makes the determination of  $g_{HHH}$  a genuine experimental *tour de force*. Other modes, such as  $e^+e^- \rightarrow HHb\bar{b}$ , have also been recently proposed<sup>50</sup> but signal yields are too small to provide any precise data. Operating at  $\sqrt{s} = 0.5$  TeV the ILC can measure the  $HHZ$  production cross section to about 15% accuracy, if the Higgs boson mass is 120 GeV, corresponding to a fractional accuracy on  $g_{HHH}$  of 23%.<sup>51</sup> Improvements can be obtained first by introducing observables sensitive to the presence of the triple Higgs vertex and then by performing the analysis at higher energies where the  $HH\nu\bar{\nu}$  channel contributes.<sup>52</sup> In the  $HHZ$  process events from diagrams containing the  $HHH$  vertex exhibit a lower invariant mass of the  $HH$  system compared to double-Higgstrahlung events. When

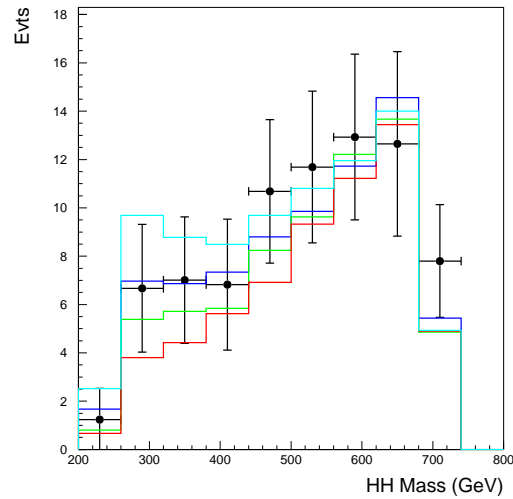


Fig. 1.9. Invariant mass of the  $HH$  system in  $e^+e^- \rightarrow HHZ$  events reconstructed with  $1 \text{ ab}^{-1}$  of data at 0.8 TeV. The histograms show the predicted distribution for various values of  $g_{HHH}$  demonstrating that the low mass region is sensitive to the contribution of the triple Higgs vertex.

the  $M_{HH}$  spectrum is fitted, a relative statistical accuracy of  $\pm 0.20$  can be obtained with  $1 \text{ ab}^{-1}$  at  $\sqrt{s} = 0.5 \text{ TeV}$ . The availability of beam polarization increases the  $HHZ$  cross section by a factor of two and that for  $HH\nu\bar{\nu}$  by a factor of four, thus offering a further possible significant improvement to the final accuracy. The ILC and, possibly, a multi-TeV  $e^+e^-$  collider represent a unique opportunity for carrying out this fundamental measurement. In fact, preliminary studies show that, the analysis of double Higgs production at the LHC is only possible after a luminosity upgrade and, even then, beyond the observation of double Higgs production, it would provide only a very limited information on the triple-Higgs coupling<sup>53,54</sup>.

#### 1.4.2. Understanding Dark Matter at the ILC

The search for new physics beyond the Standard Model has a central role in the science program of future colliders. It is instructive to contrast the LHC and the ILC in terms of their potential in such searches. Running

Table 1.2. Summary of the accuracies on the determination of the Higgs boson profile at the ILC. Results are given for a 350-500 GeV ILC with  $\mathcal{L}=0.5 \text{ ab}^{-1}$ . Further improvements, expected from a 1 TeV ILC are also shown for some of the measurements.

	$M_H$ (GeV)	$\delta(X)/X$	
		ILC-500 0.5 $\text{ab}^{-1}$	ILC-1000 1 $\text{ab}^{-1}$
$\delta M_H/M$	120-180	$(3-5) \times 10^{-4}$	
$\delta \Gamma_{tot}/\Gamma$	120-200	0.03- -   0.03 - 0.05	
$\delta g_{HWW}/g$	120-240	0.01-0.03   0.01 - 0.01	
$\delta g_{HZZ}/g$	120-240	0.01-0.05	
$\delta g_{Htt}/g$	120-200	0.02- -   0.06 - 0.13	
$\delta g_{Hbb}/g$	120-200	0.01-0.06   0.01 - 0.05	
$\delta g_{Hcc}/g$	120-140	0.06-0.12	
$\delta g_{H\tau\tau}/g$	120-140	0.03-0.05	
$\delta g_{H\mu\mu}/g$	120-140	0.15   0.04-0.06	
CP test	120	0.03	
$\delta g_{HHH}/g$	120	0.20   0.12	

at  $\sqrt{s} \leq 1 \text{ TeV}$  the ILC might appear to be limited in reach, somewhere within the energy domain being probed by the Tevatron and that to be accessed by LHC. And yet its potential for fully understanding the new physics, which the LHC might have manifested, and for probing the high energy frontier beyond the boundaries explored in hadron collisions is of paramount importance. There are several examples of how the ILC will be essential for understanding new physics. They address scenarios where signals of physics beyond the SM, as observed at the LHC, may be insufficient to decide on the nature of the new phenomena. One such example, which has been studied in some details, is the case of Supersymmetry and Universal Extra Dimensions (UED), two very different models of new physics leading to the very same experimental signature: fermion pairs plus missing energy. Here, the limited analytical power of the LHC may leave us undecided,<sup>56,57</sup> while a single spin measurement performed at the ILC precisely identifies the nature of the observed particles.<sup>58</sup> But the ILC capability to fully understand the implications of new physics, through fundamental measurements performed with high accuracy, is manifested also in scenarios where the LHC could observe a significant fraction of the new particle spectrum. An especially compelling example, which can be studied quan-

titatively, is offered by Supersymmetry in relation to Dark Matter (DM). Dark Matter has been established as a major component of the Universe. We know from several independent observations, including the cosmic microwave background (CMB), supernovas (SNs) and galaxy clusters, that DM is responsible for approximately 20 % of the energy density of the universe. Yet, none of the SM particles can be responsible for it and the observation of DM is likely the first direct signal of new physics beyond the SM. Several particles and objects have been nominated as candidates for DM. They span a wide range of masses, from  $10^{-5}$  eV, in the case of axions, to  $10^{-5}$  solar masses, for primordial black holes. Cosmology tells us that a significant fraction of the Universe mass consists of DM, but does not provide clues on its nature. Particle physics tells us that New Physics must exist at, or just beyond, the EW scale and new symmetries may result in new, stable particles. Establishing the inter-relations between physics at the microscopic scale and phenomena at cosmological scale will represent a major theme for physics in the next decades. The ILC will be able to play a key role in elucidating these inter-relations. Out of these many possibilities, there is a class of models which is especially attractive since its existence is independently motivated and DM, at about the observed density, arises naturally. These are extensions of the SM, which include an extra symmetry protecting the lightest particle in the new sector from decaying into ordinary SM states. The lightest particle becomes stable and can be chosen to be neutral. Such a particle is called a weakly interacting massive particle (WIMP) and arises in Supersymmetry with conserved R-parity (SUSY) but also in Extra Dimensions with KK-parity (UED).<sup>66</sup> Current cosmological data, mostly through the WMAP satellite measurements of the CMB, determine the DM density in the Universe with a 6 % relative accuracy.<sup>59</sup> By the next decade, the PLANCK satellite will push this uncertainty to  $\simeq 1$  %, or below.<sup>60</sup> Additional astrophysical data manifest a possible evidence of DM annihilation. The EGRET data show excess of  $\gamma$  emission in the inner galaxy, which has been interpreted as due to DM<sup>61</sup> and the WMAP data itself may show a signal of synchrotron emission in the Galactic center.<sup>62</sup> These data, if confirmed, may be used to further constrain the DM properties. Ground-based DM searches are also approaching the stage where their sensitivity is at the level predicted by Supersymmetry for some combinations of parameters.<sup>63</sup> The next decades promise to be a time when accelerator experiments will provide new breakthroughs and highly accurate data to gain new insights, not only on fundamental questions in particle physics, but also in cosmology, when studied alongside the

observations from satellites and other experiments. The questions on the nature and the origin of DM offer a prime example of the synergies of new experiments at hadron and lepton colliders, at satellites and ground-based DM experiments.

It is essential to study, in well defined, yet general enough, models, which are the properties of the new physics sector, such as masses and couplings, most important to determine the resulting relic density of the DM particles. Models exist which allow to link the microscopic particle properties to the present DM density in the Universe, with mild assumptions. If DM consists of WIMPs, they are abundantly produced in the very early Universe when  $T \simeq (t(\text{sec}))^{-1/2} > 100$  GeV and their interaction cross section is large enough that they were in thermal equilibrium for some period in the early universe. The DM relic density can be determined by solving the Boltzmann equation governing the evolution of their phase space number density.<sup>64</sup> It can be shown that, by taking the WMAP result for the DM relic density in units of the Universe critical density,  $\Omega_{DM} h^2$ , the thermal averaged DM annihilation cross section times the co-moving velocity,  $\langle \sigma v \rangle$ , should be  $\simeq 0.9$ . From this result, the mass of the DM candidate can be estimated as:

$$M_{DM} = \sqrt{\frac{\pi \alpha^2}{8 \langle \sigma v \rangle}} \simeq 100 \text{ GeV}. \quad (1.7)$$

A particle with mass  $M = \mathcal{O}(100 \text{ GeV})$  and weak cross section would naturally give the measured DM density. It is quite suggestive that new physics, responsible for the breaking of electro-weak symmetry, also introduce a WIMP of about that mass. In fact, in essentially every model of electroweak symmetry breaking, it is possible to add a discrete symmetry that makes the lightest new particle stable. Often, this discrete symmetry is required for other reasons. For example, in Supersymmetry, the conserved  $R$  parity is needed to eliminate rapid proton decay. In other cases, such as models with TeV-scale extra dimensions, the discrete symmetry is a natural consequence of the underlying geometry.

Data on DM density already set rather stringent constraints on the parameters of Supersymmetry, if the lightest neutralino  $\chi_1^0$  is indeed responsible for saturating the amount of DM observed in the Universe. It is useful to discuss the different scenarios, where neutralino DM density is compatible with the WMAP result, in terms of parameter choices in the context of the constrained MSSM (cMSSM), to understand how the measurements that the ILC provides can establish the relation between new physics and

DM. The cMSSM reduces the number of free parameters to just five: the common scalar mass,  $m_0$ , the common gaugino mass,  $m_{1/2}$ , the ratio of the vacuum expectation values of the two Higgs fields,  $\tan\beta$ , the sign of the Higgsino mass parameter,  $\mu$ , and the common trilinear coupling,  $A_0$ . It is a remarkable feature of this model that, as these parameters, defined at the unification scale, are evolved down to lower energies, the electroweak symmetry is broken spontaneously and masses for the  $W^\pm$  and  $Z^0$  bosons generated automatically. As this model is simple and defined by a small number of parameters, it is well suited for phenomenological studies. The cosmologically interesting regions in the  $m_0 - m_{1/2}$  parameter plane are shown in Figure 1.10. As we move away from the bulk region, at small values of  $m_0$  and  $m_{1/2}$ , which is already severely constrained by LEP-2 data, the masses of supersymmetric particles increase and so does the dark matter density. It is therefore necessary to have an annihilation process, which could efficiently remove neutralinos in the early universe, to restore the DM density to the value measured by WMAP. Different processes define three main regions: i) the focus point region, where the  $\chi_1^0$  contains an admixture of the supersymmetric partner of a neutral Higgs boson and annihilates to  $W^+W^-$  and  $Z^0Z^0$ , ii) the co-annihilation region, where the lightest slepton has a mass very close to  $M_{\chi_1^0}$ , iii) the  $A$  annihilation funnel, where  $M(\chi_1^0)$  is approximately half that of the heavy  $A^0$  Higgs boson, providing efficient  $s$ -channel annihilation,  $\chi\chi \rightarrow A$ . In each of these regions, researchers at the ILC will be confronted with several different measurements and significantly different event signatures.

Table 1.3. cMSSM parameters of benchmark points

Point	$m_0$	$m_{1/2}$	$\tan\beta$	$A_0$	$Sgn(\mu)$	$M(t)$
LCC1	100	250	10	-100	+	178
LCC2	3280	300	10	0	+	175
LCC3	210	360	40	0	+	178
LCC4	380	420	53	0	+	178

It is interesting to observe that the DM constraint, reduces the dimensionality of the cMSSM plane, by one unit, since the allowed regions are tiny lines in the  $m_0 - m_{1/2}$  plane, evolve with  $\tan\beta$  and depend only very weakly on  $A_0$ .<sup>65</sup> Representative benchmark points have been defined and their parameters are summarised in Table 1.3. Even though these points have been defined in a specific supersymmetric model, their phenomenol-

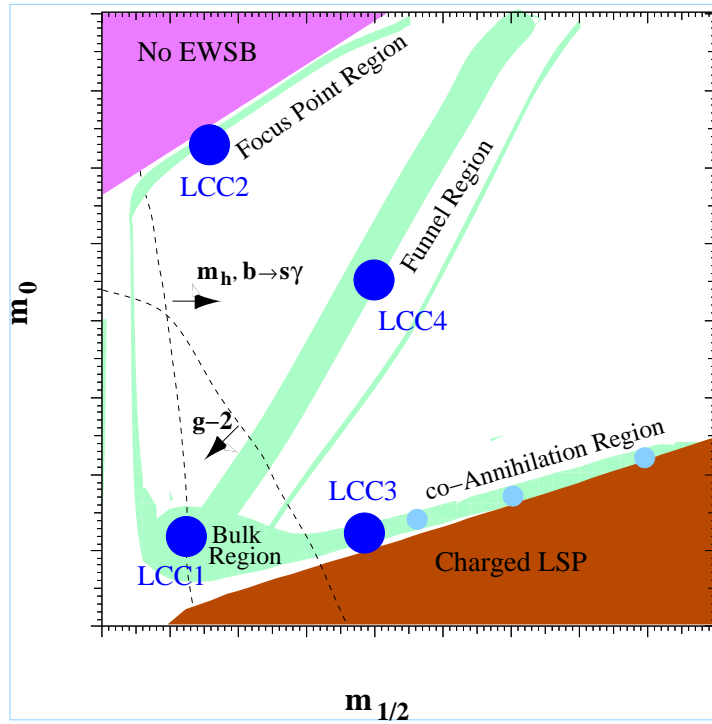


Fig. 1.10. The DM-favoured regions in the  $m_0 - m_{1/2}$  plane of the cMSSM and existing constraints. The precise locations of these regions vary with the  $\tan\beta$  parameter and therefore the axis are given without units. The indicative locations of the four benchmark points adopted, are also given. Lower limits on the Higgs boson mass and, in a portion of the parameter space, the measurement of the  $b \rightarrow s\gamma$  decay branching fraction, exclude the region at low values of  $m_{1/2}$ . A discrepancy of the measured anomalous magnetic moment of the muon value with the SM prediction would favour the region on the left of the curve labeled  $g - 2$ .

ogy is common to the more general supersymmetric solutions and we shall soon discuss the extension of results derived in this constrained model to the general MSSM. There are several features which are common to all these regions. First, the relic density depends on the mass of the lightest neutralino and of few additional particles, close in mass to it. The heavier part of the SUSY spectrum decouples from the value of  $\Omega_\chi h^2$ . This is of particular importance for the ILC. Running at  $\sqrt{s} \leq 1$  TeV, the ILC will not be able to study supersymmetric particles exceeding  $\simeq 450$ - $490$  GeV, in particular scalar quarks and heavy Higgs bosons in some regions of the parameter phase space. But, independently of the LHC results, the ILC



will either observe and measure these particles if they may be relevant to determine the relic DM density, or it will set bounds that ensure their decoupling. A second important observation is that  $\Omega_\chi h^2$  typically depends on SUSY parameters which can be fixed by accurate measurements of particle masses, particle mass splittings, decay branching fractions and production cross sections. In some instances the availability of polarised beams is advantageous. The LHC can often make precise measurements of some particles, but it is difficult for the LHC experiments to assemble the complete set of parameters needed to reconstruct annihilation cross section. It is also typical of supersymmetry spectra to contain light particles that may be very difficult to observe in the hadron collider environment. The ILC, in contrast, provides just the right setting to obtain both types of measurements. Again, it is not necessary for the ILC to match the energy of the LHC, only that it provides enough energy to see the lightest charged particles of the new sector.

Rather detailed ILC analyses of the relevant channels for each benchmark point have been performed,<sup>67-70</sup> based on parametric simulation, which includes realistic detector performances and effects of the ILC beam characteristics. It has been assumed that the ILC will be able to provide collisions at centre-of-mass energies from 0.3 TeV to 0.5 TeV with an integrated luminosity of  $500 \text{ fb}^{-1}$  in a first phase of operation and then its collision energy can be raised to 1 TeV to provide an additional data set of  $1 \text{ ab}^{-1}$ , corresponding to an additional three to four years of running. Results are summarised in terms of the estimated accuracies on masses and mass differences in Table 1.4.

In order to estimate the implications of these ILC measurements on the estimation of neutralino dark DM density  $\Omega_\chi h^2$ , broad scans of the multi-parameter supersymmetric phase space need to be performed. For each benchmark point, the soft parameters (masses and couplings) at the electroweak scale can be computed with the full 2-loop renormalization group equations and threshold corrections using *Isajet 7.69*.<sup>71</sup> Supersymmetric loop corrections to the Yukawa couplings can also be included. The electroweak-scale MSSM parameters are extracted from the high scale *cMSSM* parameters. The dark matter density  $\Omega_\chi h^2$  can be estimated using the *DarkSUSY*<sup>72</sup> and *Micromegas*<sup>73</sup> programs. These programs use the same *Isajet* code to determine the particle spectrum and couplings, including the running Yukawa couplings, and compute the thermally averaged cross section for neutralino annihilation, including co-annihilation and solve the equation describing the evolution of the number density for the DM candi-

Table 1.4. Summary of the accuracies (in GeV) on the main mass determinations by the ILC at 0.5 TeV for the four benchmark points. Results in [] brackets also include ILC data at 1 TeV.

Observable	LCC1	LCC2	LCC3	LCC4
$\delta M(\tilde{\chi}_1^0)$	$\pm 0.05$	$\pm 1.0$	$\pm 0.1$	$[\pm 1.4]$
$\delta M(\tilde{e}_R)$	$\pm 0.05$	-	$[\pm 1.0]$	$[\pm 0.6]$
$\delta M(\tilde{\tau}_1)$	$\pm 0.3$	-	$\pm 0.5$	$\pm 0.9$
$\delta M(\tilde{\tau}_2)$	$\pm 1.1$	-	-	-
$\delta(M(\mu_R) - M(\tilde{\chi}_1^0))$	$\pm 0.2$	-	$[\pm 0.2]$	$\pm 0.6$
$\delta(M(\tilde{\tau}_1) - M(\tilde{\chi}_1^0))$	0.3	-	$\pm 1.0$	$\pm 1.0$
$\delta(M(\tilde{\tau}_2) - M(\tilde{\chi}_1^0))$	$\pm 1.1$	-	$[\pm 3.0]$	-
$\delta(M(\tilde{\chi}_2^0) - M(\tilde{\chi}_1^0))$	$\pm 0.07$	$\pm 0.3$	$\pm 0.6$	$[\pm 1.8]$
$\delta(M(\tilde{\chi}_3^0) - M(\tilde{\chi}_1^0))$	$\pm 4.0$	$\pm 0.2$	$[\pm 2.0]$	$[\pm 2.0]$
$\delta(M(\tilde{\chi}_1^+) - M(\tilde{\chi}_1^0))$	$\pm 0.6$	$\pm 0.25$	$[\pm 0.7]$	$\pm 2.0$
$\delta(M(\tilde{\chi}_2^+) - M(\tilde{\chi}_1^+))$	$[\pm 3.0]$	-	$[\pm 2.0]$	$\pm 2.0$
$\delta M(A^0)$	$[\pm 1.5]$	-	$[\pm 0.8]$	$[\pm 0.8]$
$\delta \Gamma(A^0)$	-	-	$[\pm 1.2]$	$[\pm 1.2]$

date. While the assumptions of the cMSSM are quite helpful for defining a set of benchmark points, the cMSSM is not representative of the generic MSSM, since it implies several mass relations, and its assumptions have no strong physics justification. Therefore, in studying the accuracy on  $\Omega_\chi h^2$ , the full set of MSSM parameters must be scanned in an uncorrelated way and the mass spectrum evaluated for each parameter set. A detailed study has recently been performed.<sup>74</sup> I summarise here some of the findings, Table 1.5 gives results for the neutralino relic density estimates in MSSM for the LHC, the ILC at 0.5 TeV and the ILC at 1 TeV.

The LCC1 point is in the bulk region and the model contains light sleptons, with masses just above that of the lightest neutralino. The most important annihilation reactions are those with t-channel slepton exchange. At the LHC, many of the SUSY spectrum parameters can be determined from kinematic constraints. At the ILC masses can be determined both by the two-body decay kinematics of the pair-produced SUSY particles and by dedicated threshold scans. Let us consider the two body decay of a scalar quark  $\tilde{q} \rightarrow q\chi_1^0$ . If the scalar quarks are pair produced  $e^+e^- \rightarrow \tilde{q}\tilde{q}$ ,  $E_{\tilde{q}} = E_{beam}$  and the  $\chi_1^0$  escapes undetected, only the  $q$  (and the  $\tilde{q}$ ) are observed in the detector. In a 1994 paper, J. Feng and D. Finnell<sup>75</sup> pointed out that the minimum and maximum energy of production for the quark can be related to the mass difference between the scalar quark  $\tilde{q}$  and the  $\chi_1^0$ :

$$E_{max, min} = \frac{E_{beam}}{2} \left(1 \pm \sqrt{1 - \frac{m_{\tilde{q}}^2}{E_{beam}^2}}\right) \left(1 - \frac{m_{\chi}^2}{m_{\tilde{q}}^2}\right). \quad (1.8)$$

The method can also be extended to slepton decays  $\tilde{\ell} \rightarrow \ell \chi_1^0$ , which share the same topology, and allows to determine slepton mass once that of the neutralino is known or determine a relation between the masses and get  $m_{\chi_1^0}$  if that of the slepton can be independently measured. The measurement requires a precise determination of the endpoint energies of the lepton momentum spectrum,  $E_{min}$  and  $E_{max}$ . It can be shown that accuracy is limited by beamstrahlung, affecting the knowledge of  $E_{beam}$  in the equation above, more than by the finite momentum resolution,  $\delta p/p$  of the detector. The ILC has a second, and even more precise, method for mass

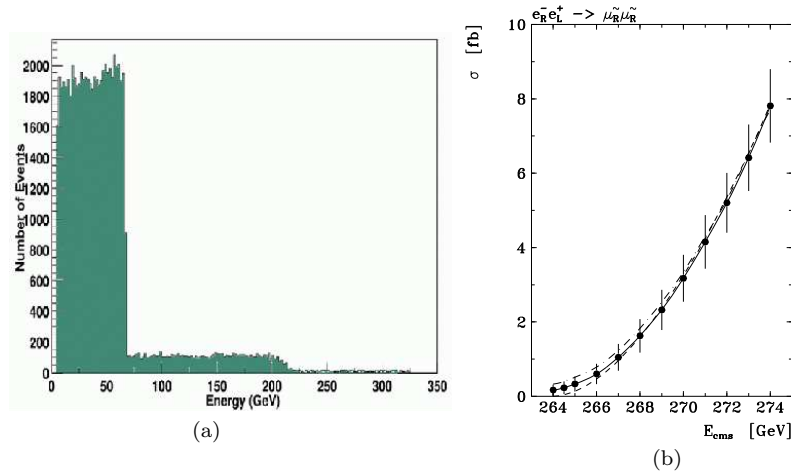


Fig. 1.11. Mass reconstruction at ILC: (a) momentum endpoint in  $\tilde{\mu} \rightarrow \mu \chi_1^0$  (from Ref.<sup>76</sup>) and (b) threshold scan for  $e^+e^- \rightarrow \tilde{\mu}^+ \tilde{\mu}^-$  (from Ref.<sup>23</sup>)

measurements. The possibility to precisely tune the collision energy allows to perform scans of the onset of the cross section for a specific SUSY particle pair production process. The particle mass and width can be extracted from a fit to the signal event yield as function of  $\sqrt{s}$ . The accuracy depends rather weakly on the number of points,  $N$ , adopted in the scan and it appears that concentrating the total luminosity at two or three different energies close to the threshold is optimal.<sup>77,78</sup> The mass accuracy,  $\delta m$  can be parametrised as:

$$\delta m \simeq \Delta E \frac{1 + 0.36/\sqrt{N}}{\sqrt{18NL\sigma}} \quad (1.9)$$

for S-wave processes, where the cross section rises as  $\beta$  and as

$$\delta m \simeq \Delta E \frac{1}{N^{1/4}} \frac{1 + 0.38/\sqrt{N}}{\sqrt{2.6NL\sigma}} \quad (1.10)$$

for P-wave processes, where the cross section rises as  $\beta^3$ . The combination of these measurements allows the ILC to determine the  $\chi_1^0$  mass to  $\pm 0.05$  GeV, which is two orders of magnitude better than the anticipated LHC accuracy, while the mass difference between the  $\tilde{\tau}_1$  and the  $\chi_1^0$  can be measured to  $\pm 0.3$  GeV, which is more than a factor ten better. Extension of ILC operation to 1 TeV gives access to the  $e^+e^- \rightarrow H^0 A^0$  process. As a result of the precision of these measurements, the ILC data at 0.5 TeV will allow to predict the neutralino relic density to  $\pm 2$  % and the addition of 1.0 TeV data will improve it to  $\pm 0.25$  %. It is suggestive that this accuracy is comparable, or better, than that expected by the improved CMB survey by the PLANCK mission. For comparison, the LHC data should provide a  $\pm 7$  % accuracy. This already a remarkable result, due the fact that, a large number of measurements will be available at the LHC and SUSY decay chains can be reconstructed. Still, the overall mass scale remains uncertain at the LHC. The direct mass measurements on the ILC data remove this uncertainty.

The LCC1 point is characterised by the relatively low SUSY mass scale, most of the particles can be observed at the LHC and their masses accurately measured at the ILC. However, in more general scenarios, the information available from both collider will be more limited. This is the case at the LCC2 point, located in the focus point region, where masses of scalar quarks, sleptons and heavy Higgs bosons are very large, typically beyond the ILC but also the LHC reach, while gauginos masses are of the order of few hundreds GeV, thus within the kinematical domain of the ILC. In this specific scenario, the LHC will observe the SUSY process  $\tilde{g} \rightarrow q\bar{q}\chi$  and the subsequent neutralino and chargino decays. Still the neutralino relic density can only be constrained within  $\pm 40$ % and the hypothesis  $\Omega_\chi h^2 = 0$ , namely that the neutralino does not contribute to the observed dark matter density in the universe, cannot be ruled out, based only on LHC data. At a 0.5 TeV collider, the main SUSY reactions are  $e^+e^- \rightarrow \chi_1^+\chi_1^-$  and  $e^+e^- \rightarrow \chi_2^0\chi_3^0$ . Operation at 1 TeV gives access also to  $e^+e^- \rightarrow \chi_2^+\chi_2^-$  and

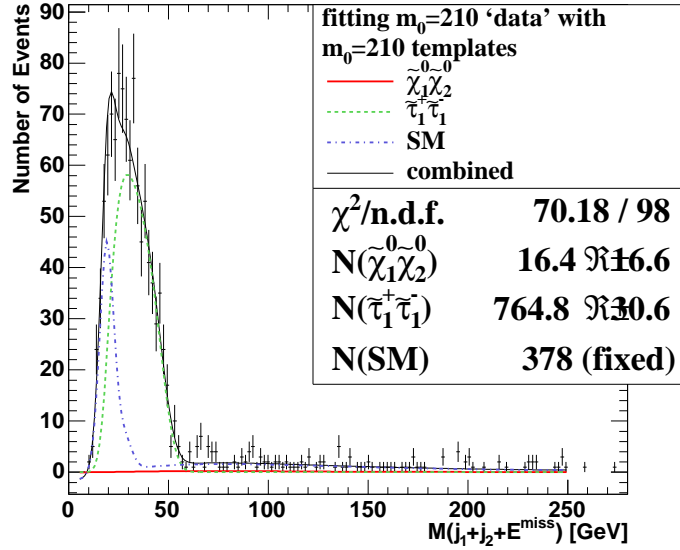


Fig. 1.12. DM-motivated SUSY  $\tilde{\tau}$  reconstruction at ILC: determination of the stau-neutralino mass difference from a reconstruction of  $e^+e^- \rightarrow \tilde{\tau}_1^+ \tilde{\tau}_1^-$  at 0.5 TeV for LCC3 (from Ref.<sup>69</sup>).

$e^+e^- \rightarrow \chi_3^0 \chi_4^0$ . Not only the gaugino mass splittings but also the polarised neutralino and chargino production cross section can be accurately determined at the ILC.<sup>68</sup> These measurements fix the gaugino-Higgsino mixing angles, which play a major role in determining the neutralino relic density. The decoupling of the heavier, inaccessible part of the SUSY spectrum, can be insured with the data at the highest energy. The combined ILC data at 0.5 TeV and 1 TeV provide an estimate of the neutralino relic density to  $\pm 8\%$  accuracy, which matches the current WMAP precision. The characteristics featured by the LCC2 point persist, while the SUSY masses increase, provided the gaugino-Higgsino mixing angle remains large enough. This DM-motivated region extends to SUSY masses which eventually exceed the LHC reach, highlighting an intriguing region of parameters where the ILC can still observe sizable production of supersymmetric particle, compatible with dark matter data, while the LHC may report no signals of New Physics.<sup>82</sup>

Instead, the last two points considered, LCC3 and LCC4, are representative of those regions where the neutralino relic density is determined by

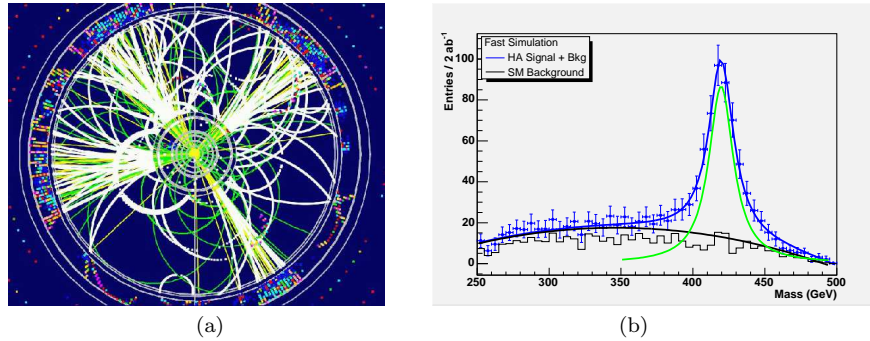


Fig. 1.13. DM-motivated SUSY Higgs reconstruction at ILC: (a) an event  $e^+e^- \rightarrow A^0 H^0 \rightarrow b\bar{b}b\bar{b}$  at 1 TeV in the LDC detector and (b) di-jet invariant mass spectrum for  $e^+e^- \rightarrow A^0 H^0 \rightarrow b\bar{b}b\bar{b}$  at 1 TeV for LCC4 (from Ref.<sup>70</sup>).

accidental relationships between particle masses. Other such regions may also be motivated by baryogenesis constraints.<sup>83</sup> The determination of the neutralino relic density, in such scenarios, depends crucially on the precision of spectroscopic measurements, due to the large sensitivity on masses and couplings. The conclusions of the current studies are that the LHC data do not provide quantitative constraints. On the contrary, the ILC can obtain interesting precision, especially when high energy data is available.

The LCC3 point is in the so-called  $\tilde{\tau}$  co-annihilation region. Here, the

Table 1.5. Summary of the relative accuracy  $\frac{\delta\Omega_\chi h^2}{\Omega_\chi h^2}$  for the four benchmark points obtained with full SUSY scans.

Benchmark Point	$\Omega h^2$	LHC	ILC 0.5 TeV	ILC 1.0 TeV
LCC1	0.192	0.072	0.018	0.024
LCC2	0.109	0.820	0.140	0.076
LCC3	0.101	1.670	0.500	0.180
LCC4	0.114	4.050	0.850	0.190

mass difference between the lightest neutralino,  $\chi_1^0$ , and the lightest scalar tau,  $\tilde{\tau}_1$ , is small enough that  $\tilde{\tau}_1 \chi_1^0 \rightarrow \tau \gamma$  can effectively remove neutralinos in the early universe. The relative density of  $\tilde{\tau}$  particles to neutralinos scales as  $e^{-\frac{m_{\tilde{\tau}} - m_\chi}{m_\chi}}$ , so this scenario tightly constrain the  $m_{\tilde{\tau}} - m_\chi$  mass difference. Here, the precise mass determinations characteristic of LCC1

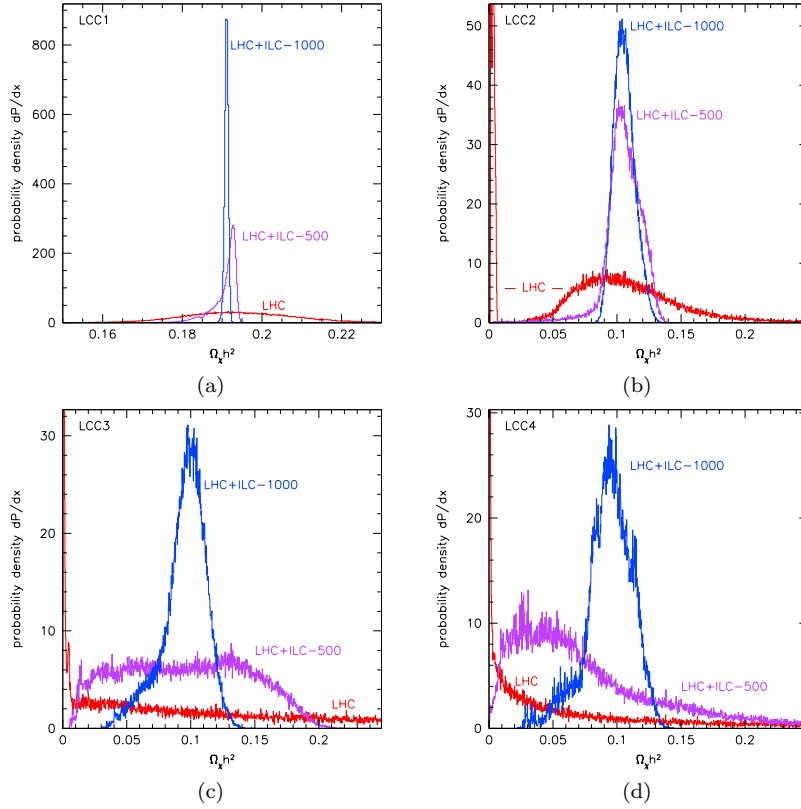


Fig. 1.14. Relic DM density determination based on simulation from LHC, ILC at 0.5 TeV and ILC at 1.0 TeV for the four SUSY benchmark points studied: a) LCC1, b) LCC2, c) LCC3 and d) LCC4. The plots show the probability density functions of the  $\Omega_h^2$  values corresponding to MSSM points compatible with the accelerator data (from Ref.<sup>74</sup>).

will not be available: at 0.5 TeV, the ILC will observe a single final state,  $\tau^+\tau^- + E_{missing}$ , from the two accessible SUSY processes,<sup>69</sup>  $e^+e^- \rightarrow \tilde{\tau}_1\tilde{\tau}_1$ ,  $\tilde{\tau} \rightarrow \tau\chi_1^0$  and  $e^+e^- \rightarrow \chi_1^0\chi_2^0$ ,  $\chi_2^0 \rightarrow \chi_1^0\tilde{\tau} \rightarrow \chi_1^0\chi_1^0\tau\tau$ . The signal topology consists of two  $\tau$ -jets and missing energy. Background processes, such as  $e^+e^- \rightarrow ZZ$  can be suppressed using cuts on event shape variables. The mass splitting can be determined by a study of the distribution of the invariant mass of the system made by the two  $\tau$ -jets and the missing energy vector,  $M_{j_1j_2E_{missing}}$ . In this variable, the remaining SM background is confined to low values and the shape and upper endpoint of the  $\tilde{\tau}_1\tilde{\tau}_1$  contri-

bution depends on the stau-neutralino mass difference,  $\Delta M = M_{\tilde{\tau}_1} - M_{\chi_1^0}$ . Templates functions can be generated for different values of  $\Delta M$  and the mass difference is extracted by a  $\chi^2$  fit of these templates to the “data”. As the  $\Delta M$  value decreases, the energy available to the  $\tau$  leptons decreases. Since  $\tau$  decays involve neutrinos, additional energy is lost from detection. When the  $\tau\tau$  system becomes soft, the four fermion background process  $ee \rightarrow ee\tau\tau$ , the so-called  $\gamma\gamma$  background which has cross sections at the nb level, makes its detection increasingly difficult. What makes possible to reject these  $\gamma\gamma$  events is the presence of the two energetic primary electrons at small angle w.r.t. the beamline.<sup>79</sup> This is a significant challenge for low angle calorimetry, since the electron has to be detected in an hostile environment populated by a large number of other electrons, of lower energy, arising from pairs created during the bunch collision.<sup>80,81</sup> A detailed study,<sup>69</sup> performed for a statistics of  $500 \text{ fb}^{-1}$ , shows that values of  $\Delta M$  as small as 5 GeV can be measured at the ILC, provided the primary electrons can be vetoed down to 17 mrad. In the specific case of the LCC3 point, where the mass splitting,  $\Delta M$ , is 10.8 GeV, an accuracy of 1 GeV can be achieved. Heavier gauginos, as well as the  $A^0$  boson, become accessible operating the ILC at 1 TeV. These data constrain both the mixing angles and  $\tan\beta$ . As a result the neutralino relic density can be estimated with an 18 % accuracy. Finally, the LCC4 point, chosen in the  $A$  funnel, has the DM density controlled by the  $\chi\chi \rightarrow A$  process. This point is rather instructive in terms of the discovery-driven evolution of a possible experimental program at the ILC. The ILC can obtain the neutralino and  $\tilde{\tau}$  masses at 0.5 TeV, following the same technique as for LCC3. We would also expect LHC experiments to have observed the  $A^0$  boson, but it is unlikely  $M_A$  could be determined accurately in  $pp$  collisions, since the available observation mode is the decay in  $\tau$  lepton pairs. At this stage, it would be apparent that the mass relation between the neutralino mass, accurately measured by the ILC at 0.5 TeV, and the  $A$  boson mass, from the LHC data, is compatible with  $M_A \simeq 2M_\chi$ , as required for the s-channel annihilation process to be effective. Three more measurements have to be performed at the ILC: the  $A^0$  mass,  $M_A$ , and width  $\Gamma_A$  and the  $\mu$  parameter, which is accessible through the mass splitting between heavier neutralinos,  $\chi_3^0, \chi_4^0$  and the lighter  $\chi_1^0, \chi_2^0$ . All these measurements are available by operating the ILC at 1 TeV.  $M_A$  and  $\Gamma_A$  can be determined by studying the  $A^0$  production in association with a  $H^0$  boson, in the reaction  $e^+e^- \rightarrow A^0H^0 \rightarrow b\bar{b}b\bar{b}$ . This process results in spectacular events with four  $b$  jets, emitted almost symmetrically, due to low energy carried by the heavy Higgs bosons (see Figure 1.13a). The cross



section, for the parameters of LCC4 corresponding to  $M_A = 419$  GeV, is just 0.9 fb highlighting the need of large luminosity at the highest energy. Jet flavour tagging and event shape analysis significantly reduces the major multi-jet backgrounds, such as  $WW$ ,  $ZZ$  and  $t\bar{t}$ . The SM  $b\bar{b}b\bar{b}$  electro-weak background has a cross section of  $\sim 3$  fb, but since it includes  $Z^0$  or  $h^0$  as intermediate states it can be efficiently removed by event shape and mass cuts. After event selection, the  $A^0$  mass and width must be reconstructed from the measured di-jet invariant masses. This is achieved by pairing jets in the way that minimises the resulting di-jet mass difference, since the masses of the  $A$  and  $H$  bosons are expected to be degenerate within a few GeV, and the di-jet masses are computed by imposing constraints on energy and momentum conservation to improve the achievable resolution and gain sensitivity to the boson natural width (see Figure 1.13b). The result is a determination of the  $A$  mass to 0.2 % and of its width to  $\simeq 15$  % if a sample of  $2 \text{ ab}^{-1}$  of data can be collected. The full set of ILC data provides a neutralino relic density evaluation with 19 % relative accuracy. The full details of how these numbers were obtained can be found in Ref.<sup>74</sup>.

SUSY offers a compelling example for investigating the complementarity in the search and discovery of new particles and in the study of their properties at the LHC and ILC. The connection to cosmology, through the study of dark matter brings precise requirements in terms of accuracy and completeness of the anticipated measurements and puts emphasis on scenarios at the edges of the parameter phase space. The interplay of satellite, ground-based and collider experiments in cosmology and particle physics will be unique and it will lead us to learn more about the structure of our Galaxy and of the Universe as well as of the underlying fundamental laws of the elementary particles. This quest will represent a major effort for science in the next several decades. The scenarios discussed above highlight the essential role of the ILC in this context. It will testing whether the particles observed at accelerators are responsible for making up a sizeable fraction of the mass of the Universe, through precision spectroscopic measurements. The data obtained at the ILC will effectively remove most particle physics uncertainties and become a solid ground for studying dark matter in our galaxy through direct and indirect detection experiments.<sup>84</sup>

#### 1.4.3. *Indirect Sensitivity to New Physics at the ILC*

Beyond Supersymmetry there is a wide range of physics scenarios invoking new phenomena at, and beyond, the TeV scale. These may explain the

origin of electro-weak symmetry breaking, if there is no light elementary Higgs boson, stabilise the SM, if SUSY is not realised in nature, or embed the SM in a theory of grand unification. The ILC, operating at high energy, represents an ideal laboratory for studying this New Physics in ways that are complementary to the LHC.<sup>85,86</sup> Not only it may directly produce some of the new particles predicted by these theories, the ILC also retains an indirect sensitivity, through precision measurements of virtual corrections to electro-weak observables, when the new particle masses exceed the available centre-of-mass energy.

One of the simplest of such SM extensions consists of the introduction of an additional  $U(1)$  gauge symmetry, as predicted in some grand unified theories.<sup>87,88</sup> The extra  $Z'$  boson, associated to the symmetry, naturally mixes with the SM  $Z^0$ . The mixing angle is already strongly constrained, by precision electroweak data, and can be of the order of few mrad at most, while direct searches at Tevatron for a new  $Z'$  boson set a lower limit on its mass around 800 GeV, which may reach 1 TeV by the time the LHC will start searching for such a state. The search for an extended gauge sector offers an interesting framework for studying the ILC sensitivity to scales beyond those directly accessible. It also raises the issue of the discrimination between different models, once a signal would be detected. The main classes of models with additional  $Z'$  bosons include  $E_6$  inspired models and left-right models (LR). In the  $E_6$  models, the  $Z'$  fermion couplings depend on the angle,  $\theta_6$ , defining the embedding of the extra  $U(1)$  in the  $E_6$  group. At the ILC, the indirect sensitivity to the mass of the new boson,  $M_{Z'}$ , can be parametrised in terms of the available integrated luminosity,  $\mathcal{L}$ , and centre-of-mass energy,  $\sqrt{s}$ . A scaling law for large values of  $M_{Z'}$  can be obtained by considering the effect of the  $Z' - \gamma$  interference in the two fermion production cross section  $\sigma(e^+e^- \rightarrow f\bar{f})$  ( $\sigma_{f\bar{f}}$  in the following). For  $s \ll M_{Z'}^2$ , and assuming the uncertainties  $\delta\sigma$  to be statistically dominated, we obtain the following scaling for the difference between the SM cross section and that in presence of the  $Z'$ , in units of the statistical accuracy:

$$\frac{|\sigma_{f\bar{f}}^{SM} - \sigma_{f\bar{f}}^{SM+Z'}|}{\delta\sigma} \propto \frac{1}{M_{Z'}^2} \sqrt{s\mathcal{L}} \quad (1.11)$$

from which we can derive that the indirect sensitivity to the  $Z'$  mass scales with the square of the centre-of-mass energy and the luminosity as:

$$M_{Z'} \propto (s\mathcal{L})^{1/4}. \quad (1.12)$$

In a full analysis, the observables sensitive to new physics contribution in

two-fermion production are the cross section  $\sigma_{f\bar{f}}$ , the forward-backward asymmetries  $A_{FB}^{f\bar{f}}$  and the left-right asymmetries  $A_{LR}^{f\bar{f}}$ . The ILC gives us the possibility to study a large number of reactions,  $e_R^+e_L^-$ ,  $e_R^+e_R^- \rightarrow (u\bar{u} + d\bar{d})$ ,  $s\bar{s}$ ,  $c\bar{c}$ ,  $b\bar{b}$ ,  $t\bar{t}$ ,  $e^+e^-$ ,  $\mu^+\mu^-$ ,  $\tau^+\tau^-$  with final states of well defined flavour and, in several cases, helicity. In order to achieve this, jet flavour tagging is essential to separate  $b$  quarks from lighter quarks and  $c$  quarks from both  $b$  and light quarks. Jet-charge and vertex-charge reconstruction allows then to tell the quark from the antiquark produced in the same event.<sup>89,90</sup> Similarly to LEP and SLC analyses, the forward-backward asymmetry can be obtained from a fit to the flow of the jet charge  $Q^{jet}$ , defined as  $Q^{jet} = \frac{\sum_i q_i |p_i T|^k}{\sum_i |p_i T|^k}$ , where  $q_i$  is the particle charge,  $p_i$  its momentum,  $T$  the jet thrust axis and the sum is extended to all the particles in a given jet. Another possible technique uses the charge of secondary particles to determine the vertex charge and thus the quark charge. The application of this technique to the ILC has been studied in some details in relation to the optimisation of the Vertex Tracker.<sup>91</sup> At ILC energies, the  $e^+e^- \rightarrow f\bar{f}$  cross sections are significantly reduced, compared to those at LEP and SLC: at 1 TeV the cross section  $\sigma(e^+e^- \rightarrow b\bar{b})$  is only 100 fb, so high luminosity is essential and new experimental issues emerge. At 1 TeV, the ILC beamstrahlung parameter doubles compared to 0.5 TeV, beam-beam effects becoming important, and the primary  $e^+e^-$  collision is accompanied by  $\gamma\gamma \rightarrow$  hadrons interactions.<sup>92</sup> Being mostly confined in the forward regions, this background may reduce the polar angle acceptance for quark flavour tagging and dilute the jet charge separation using jet charge techniques. The statistical accuracy for the determination of  $\sigma_{f\bar{f}}$ ,  $A_{FB}^{f\bar{f}}$  and  $A_{LR}^{f\bar{f}}$  has been studied, for  $\mu^+\mu^-$  and  $b\bar{b}$ , taking the ILC parameters at  $\sqrt{s} = 1$  TeV. The additional particles from the  $\gamma\gamma$  background cause a broadening of the  $Q^{jet}$  distribution and thus a dilution of the quark charge separation. Detailed full simulation and reconstruction is needed to fully understand these effects. Despite these backgrounds, the anticipated experimental accuracy in the determination of the electro-weak observables in two-fermion processes at 1 TeV is of the order of a few percent, confirming the ILC role as the precision machine. Several scenarios of new physics have been investigated.<sup>93,94</sup> The analysis of the cross section and asymmetries at 1 TeV would reveal the existence of an additional  $Z'$  boson up to  $\simeq 6$ -15 TeV, depending on its couplings. As a comparison the LHC direct sensitivity extends up to approximately 4-5 TeV. The ILC indirect sensitivity also extends to different models on new physics, such as 5-dimensional exten-

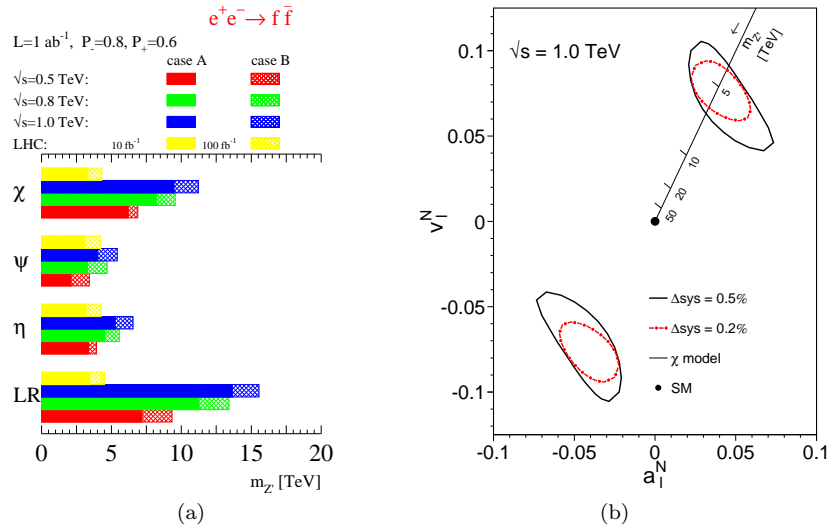


Fig. 1.15. Indirect sensitivity to  $Z'$  bosons at ILC: (a) mass sensitivity to different  $Z'$  models for  $1 \text{ ab}^{-1}$  of data at different centre-of-mass energies compared to that of LHC and (b) accuracy on leptonic couplings for a  $5 \text{ TeV}$   $Z'$  boson (from Ref.<sup>23</sup>)

sion of the SM with fermions on the boundary for a compactification where scales up to about  $30 \text{ TeV}$  can be explored. Finally, fermion compositeness or the exchange of very heavy new particles can be described in terms of effective four-fermion contact interactions.<sup>96</sup> The interaction depends on a scale  $\Lambda = M_X/g$ , where  $M_X$  is the mass of the new particle and  $g$  the coupling. Limits to this scale  $\Lambda$  can be set up to  $\simeq 100 \text{ TeV}$ , which shows that the ILC sensitivity to new phenomena can exceed its centre-of-mass energy by a significant factor. In order to maximise this indirect sensitivity to new physics, the precision of the SM predictions should match the experimental accuracy. Now, at TeV energies, well above the electroweak scale, the ILC will face the effects of large non-perturbative corrections. Large logarithms  $\propto \alpha^n \log^{2n}(M^2/s)$  arise from the exchange of collinear, soft gauge bosons and are known as Sudakov logarithms.<sup>95</sup> At  $1 \text{ TeV}$  the logarithmically enhanced  $W$  corrections to  $\sigma_{b\bar{b}}$ , of the form  $\alpha \log^2(M_W^2/s)$  and  $\alpha \log(M_W^2/s)$  amount to 19% and -4% respectively. The effect of these large logarithmic corrections has been studied in some details.<sup>17,97</sup> It will be essential to promote a program of studies to reduce these theoretical uncertainties, to fully exploit the ILC potential in these studies.

#### 1.4.4. Run Plan Scenario

One of the points of strength of the ILC is in its remarkable flexibility of running conditions. Not only the centre-of-mass energy can be changed over approximately an order of magnitude, but the beam particle and their polarization state can be varied to suit the need of the physics processes under study. At the same time, the ILC program is most diversified and data taken at the same centre-of-mass energy may be used for very different analyses, such as precise top mass determination, Higgs boson studies and reconstruction of SUSY decays. This has raised concerns whether the claimed ILC accuracies can be all achieved with a finite amount of data. A dedicated study was performed in 2001, under the guidance of Paul Granis, taking two physics scenarios with Supersymmetry realised at relatively low mass, one being the LCC1 benchmark point, rich in pair-produced particles and requiring detailed threshold scans.<sup>98</sup> The study assumes a realistic profile for the delivered luminosity, which increases from  $10 \text{ fb}^{-1}$  in the first year to  $200 \text{ fb}^{-1}$  in the fifth year and  $250 \text{ fb}^{-1}$  afterward, for a total integrated equivalent luminosity  $\int \mathcal{L} = 1 \text{ ab}^{-1}$ . The proposed run plan starts at the assumed maximum energy of 0.5 TeV for a first determination of the sparticle masses through the end-point study and then scans the relevant thresholds, including  $t\bar{t}$  in short runs with tuned polarization states. A summary is given in Table 1.6. This plan devotes approximately

Table 1.6. ILC Run plan scenario for LCC1.

Beams	$\sqrt{s}$ (TeV)	Pol.	$\int \mathcal{L}$ ( $\text{fb}^{-1}$ )	Comments
$e^+e^-$	0.500	L/R	335	Sit at max. energy for sparticle endpoint measurements
$e^+e^-$	0.270	L/R	100	Scan $\chi_1^0\chi_2^0$ (R pol.) and $\tilde{\tau}_1\tilde{\tau}_1$ (L pol.)
$e^+e^-$	0.285	R	50	Scan $\tilde{\mu}_R\tilde{\mu}_R$
$e^+e^-$	0.350	L/R	40	Scan $t\bar{t}$ , $\tilde{e}_R\tilde{e}_L$ (L & R pol.), $\chi_1^+\chi_1^-$ (L pol.)
$e^+e^-$	0.410	L/R	100	Scan $\tilde{\tau}_2\tilde{\tau}_2$
$e^-e^-$	0.285	RR	10	Scan for $\tilde{e}_R$ mass

two third of the total luminosity at, or near, the maximum energy, so the program will be sensitive to unexpected new phenomena at high energy, while providing accurate measurements of masses through dedicated scans.

## 1.5. Sensors and Detectors for the ILC

The development of the ILC accelerator components and the definition of its physics case has been paralleled by a continuing effort in detector design and sensor R&D. This effort is motivated by the need to design and construct detectors which match the ILC promise to provide extremely accurate measurements over a broad range of collision energies and event topologies. It is important to stress that, despite more than a decade of detector R&D for the LHC experiments, much still needs to be done to obtain sensors matching the ILC requirements. While the focus of the LHC-motivated R&D has been on sensor radiation hardness and high trigger rate, the ILC, with its more benign background conditions and lower interaction cross sections, admits sensors of new technology which, in turn, have better granularity, smaller thickness and much improved resolution. Sensor R&D and detector design are being carried out world-wide and are starting deploying prototype detector modules on test beamlines.

### 1.5.1. *Detector Concepts*

The conceptual design effort for an optimal detector for the ILC interaction region has probed a wide spectrum of options which span from a spherical detector structure to improved versions of more orthodox barrel-shaped detectors. These studies have been influenced by the experience with SLD at the SLC, ALEPH, DELPHI and OPAL at LEP, but also with ATLAS and CMS at the LHC. The emphasis on accurate reconstruction of the particle flow in hadronic events and thus of the energy of partons is common to all designs. The main tracker technology drives the detector designs presently being studied. Four detector concepts have emerged, named GLD, LDC, SiD and 4<sup>th</sup> Concept.<sup>99</sup> A large volume, 3D continuous tracking volume in a Time Projection Chamber is the centerpiece of the GLD, the LDC and the so-called 4<sup>th</sup> Concept designs. The TPC is followed by an highly segmented electro-magnetic calorimeter for which these three concepts are contemplating different technologies. A discrete tracker made of layers of high precision Silicon microstrip detectors, and a larger solenoidal field, which allows to reduce the radius, and thus the size, of the calorimeter is being studied in the context of the SiD design. Dedicated detector design studies are being carried out internationally<sup>100,101</sup> to optimise, through physics benchmarks,<sup>102</sup> the integrated detector concepts. Such design activities provide a bridge from physics studies to the assessment of priorities

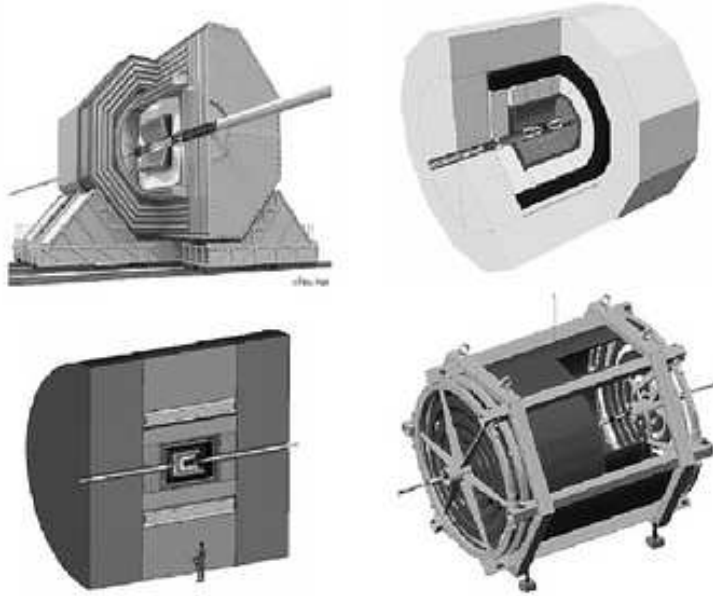


Fig. 1.16. View of the four ILC detector concepts presently being studied: GLD (upper left), LDC (upper right), SiD (lower left) and 4<sup>th</sup> Concept (lower right).

in detector R&D and are evolving towards the completion of engineered design reports at the end of this decade, synchronously with that foreseen for the ILC accelerator.

### 1.5.2. *Vertexing and Tracking*

The vertex and main tracker detectors must provide jet flavour identification and track momentum determination with the accuracy which makes the ILC such a unique facility for particle physics. The resolution in extrapolating charged particle trajectories to their production point, the so-called impact parameter, is dictated by the need to distinguish Higgs boson decays to  $c\bar{c}$  from those to  $b\bar{b}$  pairs, but also  $\tau^+\tau^-$  and gluon pairs, as discussed in section 1.4.1. In addition, vertex charge measurements put emphasis on precise extrapolation of particle tracks down to very low momenta. Tagging of events with multiple  $b$  jets, such as  $e^+e^- \rightarrow H^0 A^0 \rightarrow b\bar{b}b\bar{b}$ , discussed in section 1.4.2, underscores the need of high tagging efficiency,  $\epsilon_b$ , since

the overall efficiency scales as  $\epsilon_b^N$ , where  $N$  is the number of jets to be tagged. This is best achieved by analysing the secondary vertex structures in hadronic jets. A  $B$  meson, from a Higgs boson produced at 0.5 TeV, has an average energy of  $x_B\sqrt{s}/4 \simeq 100$  GeV, where  $x_B \simeq 0.7$  represents the average  $b$  fragmentation function, or a  $\gamma$  value of  $\simeq 70$ . Since  $c\tau \simeq 500$   $\mu\text{m}$ , the average decay distance  $\beta\gamma c\tau$  is 3.5 mm and the average impact parameter,  $\beta\gamma c\tau \sin\theta$ , is 0.5 mm. In comparison, a  $D$  meson from a  $H \rightarrow c\bar{c}$  decay has a decay length of 1.3 mm. More importantly, the average charged decay multiplicity for a  $B$  meson is 5.1, while for a  $D$  meson is 2.7. Turning these numbers into performance requirements sets the target accuracy for the asymptotic term  $a$  and the multiple scattering term  $b$  defining the track extrapolation resolution in the formula

$$\sigma_{\text{extrapolation}} = a \oplus \frac{b}{p_t} \quad (1.13)$$

The ILC target values are compared to those achieved by the DELPHI experiment at LEP, those expected for ATLAS at the LHC and the best performance ever achieved at a collider experiment, that of SLD, in Table 1.7. This comparison shows that the improvements required for ILC

Table 1.7. Values for the asymptotic term  $a$  and multiple scattering term  $b$  defining the track extrapolation resolution required for the ILC compared to those obtained by other collider experiments.

Experiment	$a$ ( $\mu\text{m}$ )	$b$ ( $\mu\text{m}/\text{GeV}$ )
ILC	5	10
DELPHI	28	65
ATLAS	15	75
SLD	8	33

on state-of-the-art technology is a factor 2-5 on asymptotic resolution and another factor 3-7 on the multiple scattering term.

At the ILC, particle tracks in highly collimated jets contribute a local track density on the innermost layer of 0.2-1.0 hits  $\text{mm}^{-2}$  at 0.5 TeV, to reach 0.4-1.5 hits  $\text{mm}^{-2}$  at 1.0 TeV. Machine-induced backgrounds, mostly pairs, add about 3-4 hits  $\text{mm}^{-2}$ , assuming that the detector integrates 80 consecutive bunch crossings in a train. These values are comparable to, or even exceed, those expected on the innermost layer of the LHC detec-



tors: 0.03 hits  $\text{mm}^{-2}$  for proton collisions in ATLAS and 0.9 hits  $\text{mm}^{-2}$  for heavy ion collisions in ALICE. Occupancy and point resolution set the pixel size to  $20 \times 20 \mu\text{m}^2$  or less. The impact parameter accuracy sets the layer material budget to  $\leq 0.15\% X_0/\text{layer}$ . This motivates the development of thin monolithic pixel sensors. Charge coupled devices (CCD) have been a prototype architecture after the success of the SLD VXD3.<sup>103</sup> However, to match the ILC requirements in terms of radiation hardness and read-out speed significant R&D is needed. New technologies, such as CMOS active pixels,<sup>104</sup> SOI<sup>105</sup> and DEPFET<sup>106</sup> sensors, are emerging as promising, competitive alternatives, supported by an intensive sensor R&D effort promoted for the ILC.<sup>107</sup>

The process  $e^+e^- \rightarrow H^0 Z^0$ ,  $H^0 \rightarrow X$ ,  $Z^0 \rightarrow \ell^+\ell^-$  gives access to Higgs production, irrespective of the Higgs decay properties. Lepton momenta must be measured very accurately for the recoil mass resolution to be limited by the irreducible smearing due to beamstrahlung. Since the centre-of-mass energy  $\sqrt{s} = E_H + E_Z$  is known and the total momentum  $p_H + p_Z = 0$ , the Higgs mass,  $M_H$  can be written as:

$$M_H^2 = E_H^2 - p_H^2 = (\sqrt{s} - E_Z)^2 - p_Z^2 = s + E_Z^2 - 2\sqrt{s}E_Z - p_Z^2 = s - 2\sqrt{s}E_Z + M_Z^2 \quad (1.14)$$

In the decay  $Z^0 \rightarrow \mu^+\mu^-$ ,  $E_Z = E_{\mu^+} + E_{\mu^-}$  so that the resolution on  $M_H$  depends on that on the muon momentum. In quantitative terms the resolution required is

$$\delta p/p^2 < 2 \times 10^{-5} \quad (1.15)$$

A comparison with the performance of trackers at LEP and LHC is given in Table 1.8. The ability to tag Higgs bosons, independent on their decay mode

Table 1.8. Values for the momentum resolution  $\delta p/p^2$  for the main tracker and the full tracking system at ILC, LEP and LHC. These values do not include the vertex constraint.

Experiment	Main Tracker Only	Full Tracker
ILC	$1.5 \times 10^{-4}$	$5 \times 10^{-5}$
ALEPH	$1.2 \times 10^{-3}$	$5 \times 10^{-4}$
ATLAS	–	$2 \times 10^{-4}$

is central to the ILC program in Higgs physics. A degraded momentum resolution would correspond to larger background, mostly from  $e^+e^- \rightarrow$

$ZZ^*$ , being accepted in the Higgs signal sample. This degrades the accuracy on the determination of the Higgs couplings both in terms of statistical and systematic uncertainties. The particle momentum is measured through its bending radius  $R$  in the solenoidal magnetic field,  $B$ . The error on the curvature,  $k = 1/R$ , for a particle track of high momentum, measured at  $N$  equidistant points with an accuracy,  $\sigma$ , over a length  $L$ , applying the constraint that it does originate at the primary vertex (as for the leptons from the  $Z^0$  in the Higgstrahlung reaction) is given by:<sup>108</sup>

$$\delta k = \frac{\sigma}{L^2} \sqrt{\frac{320}{N+4}} \quad (1.16)$$

This shows that the same momentum resolution can be achieved either by a large number of measurements, each of moderate accuracy, as in the case of a continuous gaseous tracker, or by a small number of points measured with high accuracy, as in the case of a discrete Si tracker. Continuous tracking capability over a large area, with timing information and specific ionization measurement, and its robust performance make the Time Projection Chamber an attractive option for precision tracking at the ILC. The introduction of Micro Pattern Gaseous Detectors<sup>109,110</sup> (MPGD) offers significant improvements in terms of reduced  $E \times B$ , larger gains, ion suppression and faster, narrower signals providing better space resolution. Improving on the space resolution requires an optimal sampling of the collected charge, while the high solenoidal magnetic field reduces the diffusion effects. Several paths are presently being explored with small size prototypes operated on beamlines and in large magnetic fields.<sup>111,112</sup>

A multi-layered Si strip detector tracker in an high  $B$  field may offer a competitive  $\delta p/p^2$  resolution with reduced material budget and afford a smaller radius ECAL, thus reducing the overall detector cost. This is the main rationale promoting the development of an all-Si concept for the main tracker, which follows the spirit of the design of the CMS detector at LHC. Dedicated conceptual design and module R&D is being carried out as a world-wide program.<sup>113</sup> There is also considerable R&D required for the engineering of detector ladders, addressing such issues as mechanical stability and integration of cooling and electrical services. These modules may also be considered as supplemental tracking devices in a TPC-based design to provide extra space points, with high resolution, and in end-cap tracking planes. Assessing the required detector performance involves realistic simulation and reconstruction code accounting for inefficiencies, noise, overlaps and backgrounds.

### 1.5.3. Calorimetry

The ILC physics program requires precise measurements of multi-jet hadronic events, in particular di-jet invariant masses to identify  $W$ ,  $Z$  and Higgs bosons, through their hadronic decays. An especially demanding reaction is  $e^+e^- \rightarrow Z^0 H^0 H^0$ , which provides access to the triple Higgs coupling as discussed in section 1.4.1. The large background from  $e^+e^- \rightarrow Z^0 Z^0 Z^0$  can be reduced only by an efficient  $H^0/Z^0$  separation, based on their masses. This impacts the parton energy resolution through the measurement of hadronic jets. Detailed simulation<sup>51</sup> shows that a jet energy resolution  $\frac{\sigma_{E_{jet}}}{E_{jet}} \simeq \frac{0.30}{\sqrt{E}}$  is required, in order to achieve an interesting resolution on the  $g_{HHH}$  coupling. The analysis of other processes, such as  $e^+e^- \rightarrow W^+W^-\nu\bar{\nu}$  and Higgs hadronic decays, leads to similar conclusions.<sup>115</sup> In the case of the determination of  $H^0 \rightarrow W^+W^-$  branching fractions, the statistical accuracy degrades by 22 % when changing the jet energy resolution from  $\frac{0.30}{\sqrt{E}}$  to  $\frac{0.60}{\sqrt{E}}$ . Such performance is unprecedented

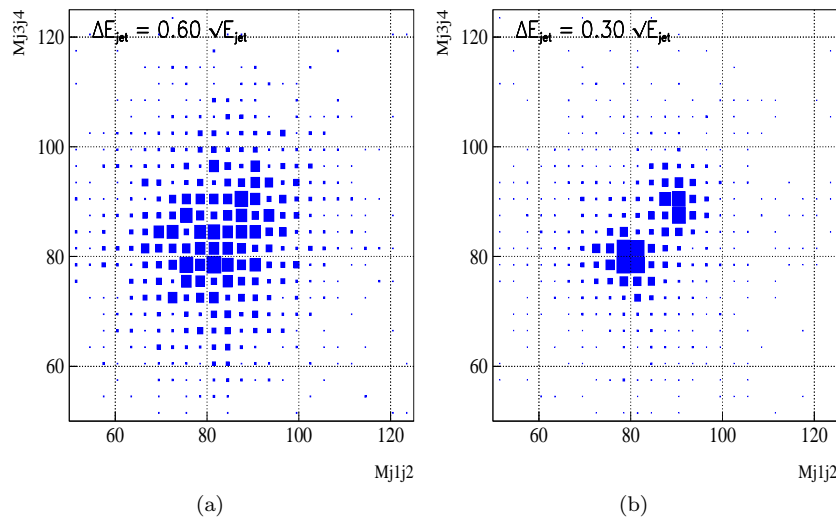


Fig. 1.17.  $W^\pm$  and  $Z^0$  gauge boson pair production separation at the ILC: invariant mass of the first di-jet pair vs. that of the second for a sample of  $WW$  and  $ZZ$  for two different assumptions on the jet energy resolution (a)  $\frac{0.30}{\sqrt{E}}$  and (b)  $\frac{0.60}{\sqrt{E}}$  (from Ref<sup>114</sup>).

and requires the development of an advanced calorimeter design as well as new reconstruction strategies. The most promising approach is based

on the *particle flow algorithm* (PFA). The energy of each particle in an hadronic jet is determined based on the information of the detector which can measure it to the best accuracy. In the case of charged particles, this is achieved by measuring the particle bending in the solenoidal field with the main tracker. Electromagnetic neutrals ( $\gamma$  and  $\pi^0$ ) are measured in the electromagnetic calorimeter and hadronic neutrals ( $K_L^0$ ,  $n$ ) in the hadronic calorimeter. The jet energy is then obtained by summing these energies:

$$E_{jet} = E_{charged} + E_{em\ neutral} + E_{had\ neutral} \quad (1.17)$$

each being measured in a specialised detector. The resolution is given by:

$$\sigma_{E_{jet}}^2 = \sigma_{charged}^2 + \sigma_{em\ neutral}^2 + \sigma_{had\ neutral}^2 + \sigma_{confusion}^2. \quad (1.18)$$

Assuming the anticipated momentum resolution,  $\sigma_E \simeq 0.11/\sqrt{E}$  for the e.m. calorimeter,  $\sigma_E \simeq 0.40/\sqrt{E}$  for the hadronic calorimeter and the fractions of charged, e.m. neutral and hadronic neutral energy in an hadronic jet we get:

$$\sigma_{charged}^2 \simeq (0.02\text{GeV})^2 \frac{1}{10} \sum \frac{E_{charged}^4}{(10\text{GeV})^4} \quad (1.19)$$

$$\sigma_{em\ neutral}^2 \simeq (0.6\text{GeV})^2 \frac{E_{jet}}{100\text{GeV}} \quad (1.20)$$

$$\sigma_{had\ neutral}^2 \simeq (1.3\text{GeV})^2 \frac{E_{jet}}{100\text{GeV}} \quad (1.21)$$

In case of perfect energy-particle association this would correspond to a jet resolution  $\simeq 0.14/\sqrt{E}$ . But a major source of resolution loss turns out to be the confusion term,  $\sigma_{confusion}$ , which originates from inefficiencies, double-counting and fakes, which need to be minimised by an efficient pattern recognition. This strategy was pioneered by the ALEPH experiment at LEP, where a resolution  $\simeq 0.60/\sqrt{E}$  was obtained, starting from the stochastic resolutions of  $\sigma_E \simeq 0.18/\sqrt{E}$  for the e.m. calorimeter, and  $\sigma_E \simeq 0.85/\sqrt{E}$  for the hadronic calorimeter.<sup>116</sup> At hadron colliders, the possible improvement from using tracking information together with calorimetric measurements is limited, due to underlying events and the shower core size. On the contrary, at the ILC these limitations can be overcome, by developing an imaging calorimeter, where spatial resolution becomes as important as energy resolution. The minimisation of the confusion rate can then be obtained by choosing a large solenoidal field,  $B$ , and calorimeter radius,  $R$ , to increase the separation between charged and neutral particles

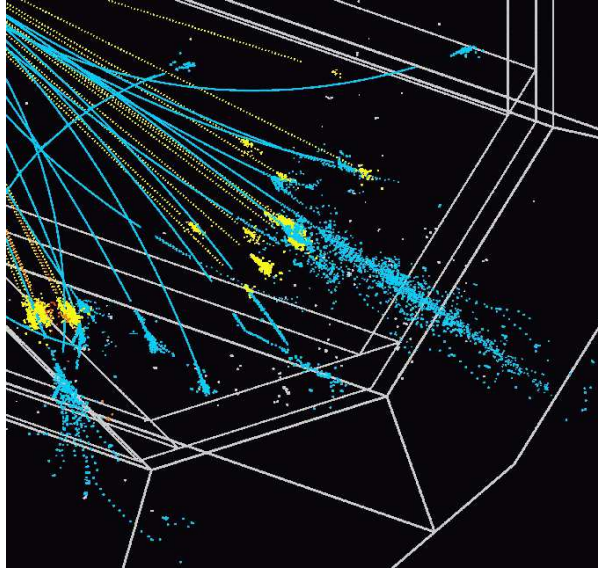


Fig. 1.18. Visualisation of the imaging calorimeter for the ILC: simulated response of a SiW calorimeter to a jet from  $e^+e^- \rightarrow W^+W^- \rightarrow jets$  at  $\sqrt{s}=0.8$  TeV.

in dense jets, a small Moliere radius,  $R_M$ , for the e.m. calorimeter, to reduce the transverse shower spread and small cells,  $R_{pixel}$ , with large longitudinal segmentation. The distance between a neutral and a charged particle, of transverse momentum  $p_t$ , at the entrance of the e.m. calorimeter located at a radius  $R$  is given by  $0.15BR^2/p_t$ , where  $B$  is the solenoidal magnetic field. A useful figure of merit of the detector in terms of the particle flow reconstruction capability is then offered by:

$$\frac{BR^2}{R_M^2 R_{pixel}^2} \quad (1.22)$$

which is a measure of the particle separation capability. The value of  $BR^2$  is limited to about  $60 \text{ Tm}^2$  by the mechanical stability. An optimal material in terms of Moliere radius is Tungsten, with  $R_M = 9$  mm. In four-jet events at  $\sqrt{s}=0.8$  TeV, there are on average 28 GeV per di-jet carried by photons, which are deposited within 2.5 cm from a charged particle at the e.m. calorimeter radius. With pixel cells of order of  $1 \times 1 \text{ cm}^2$  to ensure sufficient transverse segmentation and 30 to 40 layers in depth, the e.m. calorimeter would consist of up to 30 M channels and  $3000 \text{ m}^2$  of active Si. Due to the large amount of channels and the wish to use an absorber with the smallest

possible Moliere radius, the e.m. calorimeter is the main cost-driver of the ILC detector and its optimisation in terms of performance and cost requires a significant R&D effort. A Silicon-Tungsten calorimeter (SiW) was first proposed in the framework of the TESLA study<sup>114,117</sup> and it is currently being pursued by large R&D collaborations in both Europe and the US. Alternative technologies are also being studied by the GLD and the 4<sup>th</sup> Concept. This R&D program involves design, prototyping and tests with high energy particle beams and it is being carried out world-wide,<sup>118–120</sup> supported by efforts on detailed simulation and reconstruction.

### 1.6. Epilogue

The ILC promises to complement and expand the probe into the TeV scale beyond the LHC capabilities, matching and improving its energy reach while adding precision. Its physics program will address many of the fundamental questions of today's physics from the origin of mass, to the nature of Dark Matter. After more than two decades of intense R&D carried out world-wide, the  $e^+e^-$  linear collider, with centre-of-mass energies up to 1 TeV, has become technically feasible and a costed reference design is now available. Detectors matching the precision requirements of its anticipated physics program are being developed in an intense R&D effort carried out world-wide. Now, theoretical predictions matching the anticipated experimental accuracies are crucially needed, as well as further clues on what physics scenarios could be unveiled by signals that the LHC may soon be observing. These will contribute to further define the physics landscape for the ILC. A TeV-scale electron-positron linear collider is an essential component of the research program that will provide in the next decades new insights into the structure of space, time, matter and energy. Thanks to the efforts of many groups from laboratories and universities around the world, the technology for achieving this goal is now in hand, and the prospects for the ILC success are extraordinarily bright.

### Acknowledgments

I am grateful to the TASI organisers, in particular to Sally Dawson and Rabindra N. Mohapatra, for their invitation and the excellent organization. I am indebted to many colleagues who have shared with me both the excitement of the ILC physics studies and detector R&D, over many years, as well as many of the results included in this article. I would like

to mention here Ugo Amaldi, Timothy Barklow, Genevieve Belanger, Denis Contarato, Stefania De Curtis, Jean-Pierre Delahaye, Albert De Roeck, Klaus Desch, Daniele Dominici, John Ellis, JoAnne Hewett, Konstantin Matchev, Michael Peskin and Tom Rizzo. I am also grateful to Barry Barish, JoAnne Hewett, Mark Oreglia and Michael Peskin for reviewing the manuscript and their suggestions.

This work was supported in part by the Director, Office of Science, of the U.S. Department of Energy under Contract No.DE-AC02-05CH11231.

## References

1. M. Tigner, *Nuovo Cim.*, **37** 1228 (1965).
2. U. Amaldi, *Phys. Lett.* **B61** 313 (1976).
3. B. Richter, *IEEE Trans. Nucl. Sci.* **26**, 4261 (1979).
4. W. Schnell, *A Two Stage Rf Linear Collider Using A Superconducting Drive Linac*, CERN-LEP-RF/86-06 (1976).
5. C. r. Ahn *et al.*, *Opportunities and Requirements for Experimentation at a Very High-Energy  $e^+e^-$  Collider*, SLAC-0329 (1988).
6. G. Loew (editor), *International Linear Collider Technical Review Committee: Second Report*, SLAC-R-606 (2003).
7. [http://www.ligo.caltech.edu/~skammer/ITRP\\_Home.html](http://www.ligo.caltech.edu/~skammer/ITRP_Home.html)
8. <http://www.linearcollider.org/>
9. [http://media.linearcollider.org/rdr\\_draft\\_v1.pdf](http://media.linearcollider.org/rdr_draft_v1.pdf)
10. Report of the OECD Consultative Group on High-Energy Physics, June 2002 (<http://www.oecd.org/dataoecd/2/32/1944269.pdf>)
11. <http://www7.nationalacademies.org/bpa/EPP2010.html>
12. L. Maiani, prepared for the *9th International Symposium on Neutrino Telescopes*, Venice, Italy, 6-9 March 2001.
13. D. Treille, *Nucl. Phys. Proc. Suppl.* **109B**, 1 (2002).
14. R. Brinkmann, K. Flottmann, J. Rossbach, P. Schmueser, N. Walker and H. Weise (editors), *TESLA: The superconducting electron positron linear collider with an integrated X-ray laser laboratory. Technical design report.*, DESY-01-011B (2001).
15. R. W. Assmann *et al.*, *A 3-TeV  $e^+e^-$  linear collider based on CLIC technology*, CERN-2000-008 (2000).
16. W. Wuensch, *Progress in Understanding the High-Gradient Limitations of Accelerating Structures*, CLIC-Note-706 (2007).
17. M. Battaglia, A. De Roeck, J. Ellis and D. Schulte (editors), *Physics at the CLIC multi-TeV linear collider: Report of the CLIC Physics Working Group*, CERN-2004-005 (2004) and arXiv:hep-ph/0412251.
18. W.P. Leemans *et al.*, *Nature Physics* **2** 696 (2006).
19. B. Richter, SLAC-PUB-2854 (1981)
20. U. Amaldi, *Summary talk given at Workshop on Physics at Future Accelerators, La Thuile, Italy, Jan 7-13, 1987*, CERN-EP/87-95 (1987).

21. R. J. Noble, Nucl. Instrum. Meth. A **256**, 427 (1987).
22. H. Murayama and M. E. Peskin, Ann. Rev. Nucl. Part. Sci. **46**, 533 (1996) [arXiv:hep-ex/9606003].
23. J. A. Aguilar-Saavedra *et al.* [ECFA/DESY LC Physics Working Group], *TESLA Technical Design Report Part III: Physics at an  $e+e$ - Linear Collider*, DESY-2001-011C (2001) and arXiv:hep-ph/0106315.
24. T. Abe *et al.* [American Linear Collider Working Group], *Linear collider physics resource book for Snowmass 2001*, SLAC-R-570 (2001).
25. K. Abe *et al.* [ACFA Linear Collider Working Group], *Particle physics experiments at JLC*, KEK-REPORT-2001-11 (2001) and arXiv:hep-ph/0109166.
26. S. Dawson and M. Oreglia, Ann. Rev. Nucl. Part. Sci. **54**, 269 (2004) [arXiv:hep-ph/0403015].
27. P.W. Higgs, *Phys. Rev. Lett.* **12** 132 (1964); *idem*, *Phys. Rev.* **145** 1156 (1966); F. Englert and R. Brout, *Phys. Rev. Lett.* **13** 321 (1964); G.S. Guralnik, C.R. Hagen and T.W. Kibble, *Phys. Rev. Lett.* **13** 585 (1964).
28. A. Hasenfratz *et al.*, *Phys. Lett.* **B199** 531 (1987); M. Lüscher and P. Weisz, *Phys. Lett.* **B212** 472 (1988); M. Göckeler *et al.*, *Nucl. Phys.* **B404** 517 (1993).
29. R. Barate *et al.* [LEP Working Group for Higgs boson searches], *Phys. Lett. B* **565**, 61 (2003) [arXiv:hep-ex/0306033].
30. LEP Electroweak Working Group, Report CERN-PH-EP-2006 (2006), arXiv:hep-ex/0612034 and subsequent updates available at <http://lepewwg.web.cern.ch/LEPEWWG/>.
31. S. Heinemeyer *et al.*, arXiv:hep-ph/0511332.
32. P. Garcia-Abia, W. Lohmann and A. Raspereza, Note LC-PHSM-2000-062 (2000).
33. D. J. Miller, S. Y. Choi, B. Eberle, M. M. Muhlleitner and P. M. Zerwas, *Phys. Lett. B* **505**, 149 (2001) [arXiv:hep-ph/0102023].
34. M. Schumacher, Note LC-PHSM-2001-003 (2001).
35. A. Djouadi, M. Spira and P. M. Zerwas, *Z. Phys. C* **70**, 427 (1996) [arXiv:hep-ph/9511344].
36. M. D. Hildreth, T. L. Barklow and D. L. Burke, *Phys. Rev. D* **49**, 3441 (1994).
37. M. Carena, H. E. Haber, H. E. Logan and S. Mrenna, *Phys. Rev. D* **65**, 055005 (2002) [Erratum-ibid. *D* **65**, 099902 (2002)] [arXiv:hep-ph/0106116].
38. K. Desch, E. Gross, S. Heinemeyer, G. Weiglein and L. Zivkovic, *JHEP* **0409**, 062 (2004) [arXiv:hep-ph/0406322].
39. M. Battaglia, D. Dominici, J. F. Gunion and J. D. Wells, arXiv:hep-ph/0402062.
40. M. Battaglia, arXiv:hep-ph/9910271.
41. B. Aubert *et al.* [BABAR Collaboration], *Phys. Rev. Lett.* **93**, 011803 (2004) [arXiv:hep-ex/0404017].
42. C. W. Bauer, Z. Ligeti, M. Luke and A. V. Manohar, *Phys. Rev.* **D67**, 054012 (2003) [arXiv:hep-ph/0210027].
43. M. Battaglia *et al.*, *Phys. Lett.* **B556**, 41 (2003) [arXiv:hep-ph/0210319].
44. T. Kuhl, prepared for the *International Conference on Linear Colliders*



- (*LCWS 04*), Paris, France, 19-24 April 2004.
45. M. Battaglia and A. De Roeck, arXiv:hep-ph/0211207.
  46. M. Battaglia, arXiv:hep-ph/0211461.
  47. T. L. Barklow, arXiv:hep-ph/0312268.
  48. A. Djouadi, W. Kilian, M. Muhlleitner and P. M. Zerwas, *Eur. Phys. J.* **C10** (1999) 27 [arXiv:hep-ph/9903229].
  49. S. Kanemura, Y. Okada, E. Senaha and C. P. Yuan, *Phys. Rev. D* **70**, 115002 (2004) [arXiv:hep-ph/0408364].
  50. A. Gutierrez-Rodriguez, M. A. Hernandez-Ruiz and O. A. Sampayo, arXiv:hep-ph/0601238.
  51. C. Castanier, P. Gay, P. Lutz and J. Orloff, arXiv:hep-ex/0101028.
  52. M. Battaglia, E. Boos and W. M. Yao, in *Proc. of the APS/DPF/DPB Summer Study on the Future of Particle Physics (Snowmass 2001)* ed. N. Graf, E3016, [arXiv:hep-ph/0111276].
  53. U. Baur, T. Plehn and D. L. Rainwater, *Phys. Rev.* **D67**, 033003 (2003) [arXiv:hep-ph/0211224].
  54. U. Baur, T. Plehn and D. L. Rainwater, *Phys. Rev.* **D69**, 053004 (2004) [arXiv:hep-ph/0310056].
  55. T. L. Barklow, arXiv:hep-ph/0411221.
  56. A. Datta, K. Kong and K. T. Matchev, *Phys. Rev. D* **72**, 096006 (2005) [Erratum-ibid. *D* **72**, 119901 (2005)] [arXiv:hep-ph/0509246].
  57. J. M. Smillie and B. R. Webber, *JHEP* **0510**, 069 (2005) [arXiv:hep-ph/0507170].
  58. M. Battaglia, A. Datta, A. De Roeck, K. Kong and K. T. Matchev, *JHEP* **0507**, 033 (2005) [arXiv:hep-ph/0502041].
  59. D. N. Spergel et al. [WMAP Collaboration], *Astrophys. J. Suppl.* **148**, 175 (2003) [arXiv:astro-ph/0302209].
  60. J. R. Bond, G. Efstathiou and M. Tegmark, *Mon. Not. Roy. Astron. Soc.* **291**, L33 (1997) [arXiv:astro-ph/9702100].
  61. W. de Boer, C. Sander, V. Zhukov, A. V. Gladyshev and D. I. Kazakov, *Astron. Astrophys.* **444**, 51 (2005) [arXiv:astro-ph/0508617].
  62. D. P. Finkbeiner, arXiv:astro-ph/0409027.
  63. D. S. Akerib *et al.* [CDMS Collaboration], *Phys. Rev. Lett.* **96**, 011302 (2006) [arXiv:astro-ph/0509259].
  64. R. J. Scherrer and M. S. Turner, *Phys. Rev. D* **33**, 1585 (1986) [Erratum-ibid. *D* **34**, 3263 (1986)].
  65. M. Battaglia, A. De Roeck, J. R. Ellis, F. Gianotti, K. A. Olive and L. Pape, *Eur. Phys. J. C* **33**, 273 (2004) [arXiv:hep-ph/0306219].
  66. K. Kong and K. T. Matchev, *JHEP* **0601**, 038 (2006) [arXiv:hep-ph/0509119].
  67. G. Weiglein *et al.* [LHC/LC Study Group], arXiv:hep-ph/0410364.
  68. R. Gray *et al.*, arXiv:hep-ex/0507008.
  69. V. Khotilovich, R. Arnowitt, B. Dutta and T. Kamon, *Phys. Lett. B* **618**, 182 (2005) [arXiv:hep-ph/0503165].
  70. M. Battaglia, arXiv:hep-ph/0410123.
  71. F. E. Paige, S. D. Protopescu, H. Baer and X. Tata, arXiv:hep-ph/0312045.

72. P. Gondolo, J. Edsjo, P. Ullio, L. Bergstrom, M. Schelke and E. A. Baltz, JCAP **0407**, 008 (2004) [arXiv:astro-ph/0406204].
73. G. Belanger, F. Boudjema, A. Pukhov and A. Semenov, arXiv:hep-ph/0607059.
74. E. A. Baltz, M. Battaglia, M. E. Peskin and T. Wizansky, Phys. Rev. D **74**, 103521 (2006) [arXiv:hep-ph/0602187].
75. J. L. Feng and D. E. Finnell, Phys. Rev. D **49**, 2369 (1994) [arXiv:hep-ph/9310211].
76. G. A. Moortgat-Pick *et al.*, arXiv:hep-ph/0507011, based on work of U. Nauenberg *et al.*
77. G. A. Blair, in *Proc. of the APS/DPF/DPB Summer Study on the Future of Particle Physics (Snowmass 2001)* ed. N. Graf, E3019.
78. H. U. Martyn and G. A. Blair, Note LC-TH-2000-023.
79. P. Bambade, M. Berggren, F. Richard and Z. Zhang, arXiv:hep-ph/0406010.
80. P. Chen and V. I. Telnov, Phys. Rev. Lett. **63**, 1796 (1989).
81. T. Tsuchi, K. Yokoya and P. Chen, Part. Accel. **41**, 29 (1993).
82. H. Baer, A. Belyaev, T. Krupovnickas and X. Tata, JHEP **0402**, 007 (2004) [arXiv:hep-ph/0311351].
83. C. Balazs, M. Carena and C. E. M. Wagner, Phys. Rev. D **70**, 015007 (2004) [arXiv:hep-ph/0403224].
84. J. L. Feng, in *Proc. of the 2005 Int. Linear Collider Workshop (LCWS 2005)*, Stanford, California, 18-22 Mar 2005, pp 0013 and [arXiv:hep-ph/0509309].
85. M. Battaglia *et al.*, in *Physics and Experiments with Future Linear  $e^+e^-$  Colliders*, (A. Para and H.E. Fisk editors), AIP Conference Proceedings, New York, 2001, 607 [arXiv:hep-ph/0101114].
86. D. Dominici, arXiv:hep-ph/0110084.
87. J. L. Hewett, arXiv:hep-ph/9308321.
88. T. G. Rizzo, arXiv:hep-ph/0610104.
89. K. Ackerstaff *et al.* [OPAL Collaboration], Z. Phys. C **75**, 385 (1997).
90. K. Abe *et al.* [SLD Collaboration], Phys. Rev. Lett. **94**, 091801 (2005) [arXiv:hep-ex/0410042].
91. S. Hillert [LCFI Collaboration], *In the Proceedings of 2005 International Linear Collider Workshop (LCWS 2005), Stanford, California, 18-22 Mar 2005, pp 0313.*
92. P. Chen, T. L. Barklow and M. E. Peskin, Phys. Rev. D **49**, 3209 (1994) [arXiv:hep-ph/9305247].
93. S. Riemann, arXiv:hep-ph/9710564.
94. M. Battaglia, S. De Curtis, D. Dominici and S. Riemann, in *Proc. of the APS/DPF/DPB Summer Study on the Future of Particle Physics (Snowmass 2001)* ed. N. Graf, E3020, [arXiv:hep-ph/0112270].
95. M. Melles, Phys. Rept. **375**, 219 (2003) [arXiv:hep-ph/0104232].
96. E. Eichten, K. D. Lane and M. E. Peskin, Phys. Rev. Lett. **50**, 811 (1983).
97. P. Ciafaloni and D. Comelli, Phys. Lett. B **476**, 49 (2000) [arXiv:hep-ph/9910278].
98. M. Battaglia *et al.*, in *Proc. of the APS/DPF/DPB Summer Study on the Future of Particle Physics (Snowmass 2001)* ed. N. Graf, E3006,

- [arXiv:hep-ph/0201177].
99. <http://physics.uoregon.edu/~lc/wwstudy/concepts/>
  100. T. Behnke, *In the Proceedings of 2005 International Linear Collider Workshop (LCWS 2005), Stanford, California, 18-22 Mar 2005, pp 0006.*
  101. K. Abe *et al.* [GLD Concept Study Group], arXiv:physics/0607154.
  102. M. Battaglia, T. Barklow, M. Peskin, Y. Okada, S. Yamashita and P. Zerwas, *In the Proceedings of 2005 International Linear Collider Workshop (LCWS 2005), Stanford, California, 18-22 Mar 2005, pp 1602* [arXiv:hep-ex/0603010].
  103. T. Abe [SLD Collaboration], Nucl. Instrum. Meth. A **447** (2000) 90 [arXiv:hep-ex/9909048].
  104. R. Turchetta *et al.*, Nucl. Instrum. Meth. A **458** (2001) 677.
  105. J. Marczewski *et al.*, Nucl. Instrum. Meth. A **549** (2005) 112.
  106. R. H. Richter *et al.*, Nucl. Instrum. Meth. A **511** (2003) 250.
  107. M. Battaglia, Nucl. Instrum. Meth. A **530**, 33 (2004) [arXiv:physics/0312039].
  108. W.-M. Yao *et al.*, J. Phys. G **33**, 1 (2006)
  109. Y. Giomataris, P. Rebourgeard, J. P. Robert and G. Charpak, Nucl. Instrum. Meth. A **376**, 29 (1996).
  110. F. Sauli, Nucl. Instrum. Meth. A **386**, 531 (1997).
  111. S. Kappler *et al.*, IEEE Trans. Nucl. Sci. **51**, 1039 (2004).
  112. P. Colas *et al.*, Nucl. Instrum. Meth. A **535**, 506 (2004).
  113. J. Kroseberg *et al.*, arXiv:physics/0511039.
  114. T. Behnke, S. Bertolucci, R. D. Heuer and R. Settles, *TESLA Technical design report. Pt. 4: A detector for TESLA DESY-01-011* (2001).
  115. J. C. Brient and H. Videau, in *Proc. of the APS/DPF/DPB Summer Study on the Future of Particle Physics (Snowmass 2001)* ed. N. Graf, E3047, [arXiv:hep-ex/0202004].
  116. D. Buskulic *et al.* [ALEPH Collaboration], Nucl. Instrum. Meth. A **360**, 481 (1995).
  117. H. Videau, *Prepared for 5th International Linear Collider Workshop (LCWS 2000), Fermilab, Batavia, Illinois, 24-28 Oct 2000*
  118. D. Strom *et al.*, IEEE Trans. Nucl. Sci. **52**, 868 (2005).
  119. G. Mavromanolakis, *In the Proceedings of 2005 International Linear Collider Workshop (LCWS 2005), Stanford, California, 18-22 Mar 2005, pp 0906* [arXiv:physics/0510181].
  120. D. Strom *et al.*, *In the Proceedings of 2005 International Linear Collider Workshop (LCWS 2005), Stanford, California, 18-22 Mar 2005, pp 0908.*